CONFIDENTIAL

NASA Technical Memorandum 72852

Flight-Determined Longitudinal and Lateral-Directional Derivatives of the YF-12A Airplane (U)

Glenn B. Gilyard and Donald K. Hill

MAY 1978

NASA

CONFIDENTIAL

~~CONFIDENTIAL~~

NASA Technical Memorandum 72852

Flight-Determined Longitudinal and Lateral-Directional Derivatives of the YF-12A Airplane (U)

Glenn B. Gilyard
Dryden Flight Research Center
Edwards, California

and

Donald K. Hill
Lockheed California Company
Burbank, California

NASA
National Aeronautics
and Space Administration

Scientific and Technical Information Office

1978

~~CONFIDENTIAL~~

FLIGHT-DETERMINED LONGITUDINAL AND LATERAL-DIRECTIONAL DERIVATIVES OF THE YF-12A AIRPLANE

Glenn B. Gilyard
Dryden Flight Research Center

and

Donald K. Hill
Lockheed California Company

INTRODUCTION

The YF-12A aircraft (fig. 1) is being used in a joint NASA/USAF program to study various disciplines associated with high-speed aircraft, such as effects of nonstandard atmospheres (ref. 1), propulsion systems (ref. 2), stability and control, aircraft/propulsion system interactions (ref. 3), automatic flight control systems (ref. 4), and structures.

The YF-12A airplane has also been used as a test-bed for many other experiments, including a Mach 3 boundary layer study on a coldwall, a hollow cylinder that is 3.048 meters (10 feet) long and was mounted on a pylon beneath the aircraft's midsection (fig. 2, ref. 5). This study is also referred to as the coldwall experiment. Because the coldwall was expected to have a destabilizing effect, a detailed determination was made of the aircraft's stability at high Mach numbers.

In addition, during early coldwall flight testing the centerline ventral of the aircraft was lost in flight. A new ventral was designed and constructed of a new beryllium-aluminum composite, but additional flight tests were made before it was installed. Thus, it was possible to investigate the airplane's stability characteristics with the ventral on and off as well as with the coldwall on and off.

A secondary objective of the study was to document the interactions between the propulsion system and the aircraft's stability and control characteristics at high speeds (ref. 6). These interactions can then be considered in the formulation of advanced control laws for optimizing supersonic flight.

This report documents the longitudinal short period derivatives (including axial force coefficients) for flight at speeds from subsonic to Mach 3.0 with the ventral on and the coldwall off. The lateral-directional derivatives are documented for flight at speeds from subsonic to Mach 3.0 for all combinations of coldwall and ventral configurations. A detailed analysis was made of the subsonic lateral-directional derivatives for three levels of dynamic pressure with the ventral on and the coldwall off.

In addition, propulsion control derivatives which account for automatic inlet operation were determined and are documented for Mach numbers greater than 1.3 for the longitudinal data and greater than 1.9 for the lateral-directional data. Some comparisons are made with wind tunnel data, both published and unpublished.

SYMBOLS AND ABBREVIATIONS

Physical quantities in this report are given in the International System of Units (SI) and parenthetically in U.S. Customary Units. The measurements were taken in Customary Units.

a_X	longitudinal acceleration at center of gravity, g
a_Y	lateral acceleration at center of gravity, g
a_Z	normal acceleration at center of gravity, g
b	wing reference span, meters (feet)
C_l	dimensionless rolling-moment coefficient
C_m	dimensionless pitching-moment coefficient
C_n	dimensionless yawing-moment coefficient
C_X	dimensionless longitudinal-force coefficient
C_Y	dimensionless side-force coefficient
C_Z	dimensionless normal-force coefficient
$\bar{c}$	wing reference chord, meters (feet)
h_p	pressure altitude, meters (feet)

I_X, I_Y, I_Z	moments of inertia about the longitudinal, lateral, and normal body axes, respectively, kilogram-meters^2 (slug-feet^2)
I_{XZ}	product of inertia referred to the longitudinal and normal body axes, kilogram-meters^2 (slug-feet^2)
KEAS	knots equivalent airspeed, proportional to dynamic pressure
K1, K2	constants
M	free-stream Mach number
PCM	pulse code modulation
p	roll rate, degrees/second
q	pitch rate, degrees/second
r	yaw rate, degrees/second
S	wing reference area, meters^2 (feet^2)
SAS	stability augmentation system
V	velocity, meters/second (feet/second)
W	airplane gross weight, kilograms (pounds)
α	angle of attack, degrees
β	angle of sideslip, degrees
δ_a	aileron (left minus right elevon) position, degrees
δ_{bpd}	left minus right bypass door position, positive open, percent of full open
$\delta_{bpd,\,av}$	average bypass door position, positive open, percent of full open
δ_e	elevon deflection, degrees
δ_r	rudder deflection, degrees
δ_{spike}	left minus right spike position, positive forward, centimeters (inches)

θ	pitch attitude, degrees
φ	roll attitude, degrees

Subscripts:

$p, q, r, \alpha, \beta, \delta_a, \delta_{bpd}, \delta_{bpd,\,av}, \delta_e, \delta_r$	partial derivatives with respect to the subscripted variable

DESCRIPTION OF TEST AIRPLANE AND INLET CONTROL SYSTEM

Test Airplane

The YF-12A airplane is a twin-engined, delta-winged interceptor designed for long-range cruise at Mach numbers greater than 3 and altitudes above 24,400 meters (80,000 feet). The physical characteristics of the aircraft are given in reference 3.

An all-movable vertical rudder is mounted above each nacelle to provide directional stability and control. Each rudder is canted inward and pivots on a short fixed section that is attached directly to the top of the nacelle. There are three ventral fins on the bottom of the aircraft: a folding fin along the fuselage centerline and two small fixed fins on the nacelles below the two vertical rudders. A camera pod that was used to document the coldwall experiment was fastened at a bottom forward location on each nacelle for the series of flights analyzed in this report.

Two elevons on each wing, one inboard and one outboard of each nacelle, perform the combined functions of ailerons and elevators. The outboard elevon is linked to the inboard elevon.

The aircraft normally operates with a stability augmentation system (SAS) that increases both stability in the pitch and yaw axes and damping in the pitch, yaw, and roll axes. However, all maneuvers analyzed herein were performed with the SAS off in the axis or axes of interest. A complete description of the longitudinal automatic flight control system is given in reference 4.

Inlet Control System

The primary function of the inlet control system is to provide efficient inlet operation by automatically controlling inlet geometry. For efficient operation at Mach numbers greater than approximately 2.0, the terminal shock must be kept in the inlet slightly aft of the throat. The variable elements in the inlet geometry that permit the location of the terminal shock to be controlled are the position of the spike and the position of the bypass doors; both are controlled as a function of Mach number, angle of attack, normal acceleration, and angle of sideslip (fig. 3). The primary function of the translating spike is to control inlet throat area. For steady state flight at Mach numbers below 1.6, the spikes are full forward; for Mach numbers greater than 1.6, the spike schedule is nearly a linear function of Mach number.

The forward bypass doors are positioned around the circumference of the forward part of the nacelle aft of the desired terminal shock location. These doors permit the precise control of terminal shock position by rapidly regulating the amount of air ported overboard.

Both the spike and the bypass doors move the terminal shock in the more stable direction when variations are encountered in angle of attack, normal acceleration, and sideslip angle.

The forward bypass doors are of the rotary flush sliding type (ref. 2) and are controlled by means of a duct pressure ratio feedback loop (fig. 3). The desired duct pressure ratio is calculated by the inlet computer. The desired value is compared with the measured value, and the bypass doors are continuously adjusted to maintain the desired ratio. The bypass doors are closed below Mach 1.4.

A number of aft bypass doors, located in the aft part of the inlet just forward of the compressor face, are used to remove excess air from the inlet. These doors are shifted manually as a function of Mach number and therefore are not a factor in the derivative analysis.

During the short duration longitudinal maneuvers used for analysis (pullup and release), Mach number and angle of sideslip were kept fixed; therefore, the variations in spike and bypass door position were functions of changes in angle of attack and normal acceleration. Because the maneuver frequency was relatively low (as compared with the inlet control system dynamics), the spike and bypass doors moved nearly in phase with the changes in angle of attack and normal acceleration.

During the lateral-directional maneuvers used for analysis (rudder doublet or release from sideslip and aileron doublet), Mach number, angle of attack, and normal acceleration were kept fixed; therefore, the variations in spike and bypass door position were a function of angle of sideslip. As with the longitudinal maneuvers, because the maneuver frequency was low, the spike and bypass doors moved nearly in phase with changes in angle of sideslip. Reference 3 presents an analysis of the interaction between the airframe and the inlet control system during lateral-directional maneuvers.

A more complete description of the inlet and its control system can be found in reference 2.

INSTRUMENTATION

The parameters recorded during flight included elevon, rudder, forward bypass door, and spike position; pitch, yaw, and roll rate; normal, longitudinal, and lateral acceleration at the center of gravity; pitch and roll attitude; and angle of attack and sideslip. The data were recorded at 200 samples per second. Additional characteristics of the aircraft's instrumentation can be found in reference 7.

The values of angle of attack and angle of sideslip were acquired by using a pressure-sensing system mounted on the nose boom and were therefore subject to a time lag. The magnitude of the lag depended on flight condition and reached 0.5 second at Mach 3, high altitude flight (ref. 7).

Air data parameters were calculated for each maneuver from measurements made by a calibrated pitot-static nose boom probe.

TEST MANEUVERS

Pullup and release maneuvers were used to determine the short period longitudinal derivatives. The pair of maneuvers used most often to determine the lateral-directional derivatives consisted of a rudder doublet followed by an aileron doublet. However, because of other testing requirements, release-from-sideslip maneuvers were occasionally substituted for rudder doublets.

The flight conditions and aircraft configurations for which longitudinal and lateral-directional derivatives were obtained are presented in tables 1, 2, and 3. The data were obtained at preselected Mach number and altitude conditions, but no effort was made to perform maneuvers at specific gross weights or center-of-gravity locations. The moments of inertias were a function of gross weight and were determined from manufacturer's data.

The spike and bypass doors were in the automatic mode for all maneuvers except for three lateral-directional maneuver pairs above Mach 2, during which the spike and bypass doors were kept fixed. These fixed spike and bypass door maneuvers provided baseline data with which the data from the automatic inlet maneuvers could be compared to determine the effects of the propulsion system on Dutch roll damping and static stability.

DATA ANALYSIS

All the data were analyzed in body axes by using a maximum likelihood estimation program (ref. 8) at a rate of 20 samples per second. Three degrees of freedom were used for the analysis of both the longitudinal and the lateral-directional data.

In the longitudinal mode, only one maneuver was analyzed per flight condition. The parameters matched were longitudinal and normal acceleration, pitch rate, pitch attitude, angle of attack, and velocity. As stated previously, angle of attack was subject to lag; therefore, it was lightly weighted. (It might have been preferable not to match angle of attack, since lag was not corrected for, but the algorithm did not always converge without using it.) The equations used to analyze the longitudinal data are presented in reference 9.

In the lateral-directional mode, the two maneuvers at each flight condition were analyzed simultaneously. The parameters matched were lateral acceleration, yaw and roll rate, and roll attitude. The angle of sideslip measurement was not matched because of its lag characteristics and because satisfactory analysis was possible without it. The equations used to analyze the lateral-directional data are presented in reference 8.

The basic control variables were elevon, aileron, and rudder. For Mach numbers greater than 1.9 for lateral-directional analysis and 1.3 for longitudinal analysis, bypass door position was also used as a control variable, since inlet control system activity begins to play an important role in closed-loop aircraft dynamics at high Mach numbers. The spike and bypass doors were controlled by the same inputs, so their effects were not sufficiently independent to separate; therefore, only bypass door position was used as a control input. The bypass door derivatives (which also contain the effects of the spike) include all propulsion system effects that are proportional to variations in bypass door and spike motion. This includes such items as drag due to bypass door spillage and engine thrust variations.

The lateral-directional derivatives presented in the Results and Discussion section for Mach numbers greater than 1.9 were obtained by weighting the bypass door derivatives toward an a priori set of derivatives. The reasons for using the a priori values and the way in which they were selected are discussed in the appendix.

Representative examples of maneuver types and matches for the longitudinal short period mode and for the lateral-directional modes are presented in figures 4 and 5, respectively.

RESULTS AND DISCUSSION

The primary emphasis of this study was on the lateral-directional mode; however, longitudinal short period maneuvers were performed and analyzed to determine the trend of the longitudinal derivatives.

The results are presented in three parts. First and second, the longitudinal and lateral-directional derivatives are presented for the entire Mach number range at 400 knots equivalent airspeed (KEAS). Third, lateral-directional derivatives are presented for subsonic Mach numbers for three values of KEAS. All the derivatives are presented in body axis, coefficient form, and all flight data were acquired with the camera pods on.

Longitudinal Stability and Control Derivatives

Longitudinal stability and control derivatives are presented for Mach numbers from 0.7 to 3.0 in figure 6. All data were obtained at approximately the same dynamic pressure (400 KEAS) with the ventral on and the coldwall off. In addition, C_{m_α} was corrected to a 27-percent center of gravity.

In general, the derivatives vary smoothly with Mach number. The derivative C_{m_α} (fig. 6(a)) shows a normal trend with increasing Mach number, with magnitude peaking transonically and then gradually decreasing with increasing Mach number. The derivative C_{Z_α} shows a normal trend with increasing Mach number. Normally, C_{X_α} is not determined from short period maneuvers; however, the results are consistent, decreasing transonically and remaining fairly constant supersonically.

The derivatives C_{Z_q} and C_{X_q} were kept fixed at zero for all cases analyzed. The damping derivative, C_{m_q} (fig. 6(b)), which also contains $C_{m_{\dot\alpha}}$ effects, has a more varied trend, reaching a maximum magnitude at high subsonic Mach numbers.

The pitch control effectiveness derivative, $C_{m_{\delta_e}}$ (fig. 6(c)), reaches a maximum absolute value at high subsonic conditions, decreases rapidly at low supersonic conditions, and then decreases gradually with further Mach number increases. The derivatives $C_{Z_{\delta_e}}$ and $C_{X_{\delta_e}}$ are small and generally vary smoothly with Mach number. The generally positive value of $C_{X_{\delta_e}}$ is intuitively correct, since the normal trim condition is elevon up ($-\delta_e$) and any positive elevon motion tends toward a more-faired or streamlined condition.

The bypass door derivatives (fig. 6(d)), which include all propulsion system effects that are proportional to bypass door motion, were determined for Mach numbers greater than 1.3 (the derivatives were kept fixed at zero at lower Mach numbers). The derivative $C_{m_{\delta_{bpd,\,av}}}$ shows a consistent variation, increasing from Mach 1.4 to a maximum value at Mach 2.4 and then decreasing with increasing Mach number. In general, the derivative $C_{Z_{\delta_{bpd,\,av}}}$ becomes increasingly negative as Mach number increases, although there is significant scatter. The value of the derivative $C_{X_{\delta_{bpd,\,av}}}$ also decreases with increasing Mach number. The sign of $C_{X_{\delta_{bpd,\,av}}}$ is intuitively correct, since increasing bypass door opening, which is in the direction of increasing inlet stability, causes low velocity air to be dumped out of the nacelle, causing thrust reductions as well as drag increases. Flow field effects due to bypass door airflow are presented in reference 10.

The effects of the inlet geometry on the characteristics of the longitudinal derivatives were obtained from an analysis of longitudinal phugoid maneuvers at approximately Mach 3 and are presented in reference 9. Stability and control derivatives with respect to the velocity and altitude degrees of freedom were

obtained as well as the standard short period derivatives. The effect of inlet configuration on the derivatives was also determined.

Lateral-Directional Stability and Control Derivatives

Entire Mach number range. - Lateral-directional derivatives were acquired and analyzed for maneuver pairs performed at various values of KEAS for all four coldwall and ventral configurations. Sufficient data were obtained at 400 KEAS to present results from subsonic to high supersonic Mach numbers, and the data discussed in this section are for this value of KEAS.

The derivatives C_{n_β}, $C_{n_{\delta_a}}$, $C_{n_{\delta_r}}$, and $C_{n_{\delta_{bpd}}}$ are corrected to a 27-percent center of gravity throughout the flight envelope, although the effect of the correction is negligible in all except C_{n_β}.

Coldwall-off derivatives: The coldwall-off derivatives with and without the ventral and for Mach numbers from 0.7 to 3.0 are presented in figure 7. The low value of C_{n_β} with the ventral off prevented tests above Mach 2.8. In general, the derivatives vary smoothly with Mach number, although the scatter in the data is greater at subsonic and transonic conditions. Some of the scatter is due to the weakness of some maneuvers and the use of release-from-sideslip instead of rudder doublet maneuvers. The maneuver pairs at the low speed conditions were not optimum because of concern over the loads on and the flutter characteristics of the ventral and coldwall.

With the ventral off, C_{n_β} increases as transonic speeds are approached, decreases as Mach number increases to 1.6, increases slightly as Mach 2.0 is approached, and finally decreases as Mach number increases thereafter. The ventral increases C_{n_β} throughout the flight envelope, with the largest effect at subsonic conditions and a large effect from Mach 1.4 to 2.0. The effect of the ventral is fairly constant above Mach 2.0.

Three maneuver pairs were analyzed at supersonic Mach numbers ($M \approx 2.4$, 2.6, and 2.8) with the inlets fixed. The C_{n_β} associated with the inlets fixed agrees well with the automatic inlet C_{n_β} results. This good agreement implies that the analysis technique of using the bypass doors to represent the effects of the propulsion system, which is described in the appendix, is satisfactory.

Both C_{Y_β} and C_{l_β} reach maximum magnitudes in the transonic region and decrease with increasing Mach number. The ventral increases the magnitude of C_{Y_β} throughout the Mach number range and that of C_{l_β} in the subsonic region.

The derivative C_{n_p} (fig. 7(b)) is generally positive throughout the Mach number range, and the roll damping derivative, C_{l_p}, shows a generally decreasing trend with Mach number. The derivative C_{Y_p} was held fixed at zero for the analysis.

The yaw damping derivative, C_{n_r} (fig. 7(c)), is fairly well defined below Mach 2.0; however, there is considerable scatter above Mach 2.0. Automatic inlet operation is probably the major contributor to the scatter. The values of C_{n_r} from the inlet-fixed maneuvers are consistent and represent the most probable level of C_{n_r}. The derivative C_{l_r} is approximately zero throughout the Mach number range. The derivative C_{Y_r} was held fixed at zero for analysis.

The aileron effectiveness deviative, $C_{l_{\delta_a}}$ (fig. 7(d)), is well defined, peaking at approximately Mach 0.80 and then decreasing with increasing Mach number. The yawing-moment-due-to-aileron derivative, $C_{n_{\delta_a}}$, is significantly affected by the ventral in the subsonic region. Without the ventral, $C_{n_{\delta_a}}$ is adverse at low subsonic conditions, but it appears to go to zero at approximately Mach 0.95. The coefficient is slightly adverse in the low supersonic region and gradually approaches zero as Mach number increases. With the ventral on at subsonic conditions, $C_{n_{\delta_a}}$ is about double its value with the ventral off. The derivative appears to increase in magnitude as the transonic region is approached and then rapidly decrease after Mach 0.90. The side-force coefficient, $C_{Y_{\delta_a}}$, is also influenced by the ventral. At subsonic conditions with the ventral on, $C_{Y_{\delta_a}}$ is positive, whereas with the ventral off, $C_{Y_{\delta_a}}$ is essentially zero.

There is significant scatter in the rudder control derivatives in the subsonic and transonic regions (fig. 7(e)). The scatter may be due to, among other things, angle of attack variations resulting from large gross weight differences, differences in the types of maneuvers, different maneuver strengths, and differences in the location of the center of gravity; however, there may be other factors as well.

The rudder control effectiveness derivative, $C_{n_{\delta_r}}$ (fig. 7(e)), reaches a maximum absolute value transonically and then decreases with Mach number. The addition

of the ventral appears to increase the magnitude of $C_{n_{\delta_r}}$ in the subsonic region and also in the Mach 2.0 to 2.5 region. The rolling-moment-due-to-rudder derivative, $C_{l_{\delta_r}}$, is positive throughout the Mach number range with the ventral off. The addition of the ventral reduces $C_{l_{\delta_r}}$ to approximately zero at subsonic flight conditions but does not have a significant effect at supersonic conditions. The side-force-due-to-rudder derivative, $C_{Y_{\delta_r}}$, decreases with increasing Mach number and does not appear to be affected by ventral configuration.

The bypass door effectiveness derivatives, which were determined only for Mach numbers greater than 1.9, are presented in figure 7(f). The solid line in the plots represents a fairing of the preliminary analysis and was used as an a priori estimate for the final analysis. The yawing-moment-due-to-bypass-door derivative, $C_{n_{\delta_{bpd}}}$, is approximately zero at Mach 2.0 and then increases in magnitude with increasing Mach number. With the inlets operating automatically, the effect of $C_{n_{\delta_{bpd}}}$ is responsible for most of the aircraft/propulsion system interactions mentioned previously and discussed in reference 3. It should be recalled that the bypass door derivatives include the effects of spike motion. Both $C_{Y_{\delta_{bpd}}}$ and $C_{l_{\delta_{bpd}}}$ are small and near zero over the Mach number range. The ventral has no apparent effect on the bypass door derivatives.

The results of wind tunnel tests designed to determine inlet-airframe interactions at high Mach numbers are presented in reference 11.

Coldwall-off derivatives: The lateral-directional derivatives obtained with the coldwall on and the ventral off and on are presented in figure 8. One flight was also performed with an insulation cover on the coldwall, and these results are also included. There are few data below Mach 2.0, since the subject of primary interest with the coldwall on was the aircraft's static directional stability at high Mach numbers.

In general, the derivative results and trends in figure 8 are similar to those in figure 7, except for a reduction in C_{n_β} with the coldwall on. Therefore, only the effects of the coldwall on C_{n_β} are discussed. The variation of C_{n_β} with Mach number with the coldwall off and on is presented in figure 9.

With the ventral on (fig. 9(a)), the coldwall reduces C_{n_β} approximately 0.0002 over the entire high Mach number range. Wind tunnel predictions from

reference 5, which were obtained without camera pods on the nacelle, are also presented. Unpublished flight data not presented in the figure indicated that the camera pods significantly reduced C_{n_β} at Mach numbers from 2.0 to 2.8. The comparison of the flight and wind tunnel data in figure 9(a) indicates the same thing. The C_{n_β} reduction in this Mach region is thought to be due to the impingement of the shock waves from the camera pods on the centerline ventral. The wind-tunnel-predicted loss of static directional stability due to the coldwall agrees quite well with the flight-determined effect.

The effect of the coldwall on C_{n_β} is approximately the same with the ventral off (fig. 9(b)) as it is with the ventral on. An additional ventral-off configuration investigated was one with an insulation cover on the coldwall. The insulation cover has a blunted ogive nose, a cylindrical body, and a truncated base (fig. 2 and ref. 5). Static directional stability was greater with the insulation than without it for all supersonic conditions tested.

Subsonic lateral-directional derivatives. - Because a new ventral was built for the aircraft, extensive flight testing was performed at subsonic Mach numbers, where the ventral loads and flutter characteristics are most critical. Standard stability and control maneuvers were used to investigate the ventral loads and flutter characteristics. The maneuvers were also analyzed to determine aircraft stability and control derivatives. The aircraft configuration analyzed had the camera pods on, the ventral on, and the coldwall off. The flight-determined derivatives are presented in figure 10, and the flight conditions and initial aircraft conditions are presented in table 3. Data are presented for three levels of dynamic pressure (300 KEAS, 350 KEAS, and 400 KEAS). As before, the derivatives C_{n_β}, $C_{n_{\delta_a}}$, and $C_{n_{\delta_r}}$ are corrected to a 27-percent center of gravity.

A limited wind tunnel investigation was conducted to determine the ventral loads and the effect of the ventral on the aileron derivatives. (The ventral tends to act as a splitter plate between the left and right inboard elevons on the undersurface of the aft fuselage.) The resulting sideslip and aileron derivatives, previously unpublished, are included in figure 10 for comparison with the flight data. The wind tunnel data are for an angle of attack of 3°, and C_{n_β} is corrected to a 27-percent center of gravity. The camera pods were off for the wind tunnel data, whereas they were on for the flight data. Other unpublished wind tunnel data indicate that the effect of the pods on the sideslip derivatives at subsonic conditions is negligible. (Data are not available to determine the effects of the pods on the aileron derivatives.)

The trends in the subsonic derivatives in figure 10 should be interpreted with care. Although many of the derivatives (C_{l_β}, for example) seem to vary as a function of KEAS, the differences in the data are probably due primarily to the effects of angle of attack.

CONCLUDING REMARKS

Longitudinal and lateral-directional stability and control derivatives were determined from flight data for ventral-on and -off and coldwall-on and -off configurations of the YF-12A airplane by using a maximum likelihood estimation program. Camera pods were installed for all flight tests. Longitudinal derivatives are presented for Mach numbers from 0.7 to 3.0 with the ventral on and the coldwall off. Lateral-directional data are presented for Mach numbers from 0.7 to 3.0 for all combinations of ventral and coldwall configurations. A few data are presented for a configuration with an insulation cover on the coldwall.

In general, the derivatives vary smoothly with Mach number.

The centerline ventral increases the static directional stability derivative, C_{n_β}, throughout the Mach number range. The coldwall reduces C_{n_β} throughout the high Mach number range. The wind-tunnel-predicted effect of the coldwall on C_{n_β} agrees well with the flight data.

Propulsion system effects due to the variable inlet geometry were determined longitudinally for Mach numbers greater than 1.3 and lateral directionally for Mach numbers greater than 1.9.

Dryden Flight Research Center
National Aeronautics and Space Administration
Edwards, Calif., August 25, 1977

APPENDIX — USE OF A PRIORI VALUES IN DETERMINING LATERAL-DIRECTIONAL BYPASS DOOR DERIVATIVES

The automatic changes in inlet geometry have significant effects on aircraft motion at Mach numbers greater than 2.0. The most obvious effects are a reduction in damping and an increase in the frequency of the Dutch roll oscillations. If bypass door motion is not considered in a stability and control analysis, the effective value of C_{n_β} increases and the effective value of C_{n_r} decreases (and can become positive). These effects on C_{n_β} and C_{n_r} are due to the fact that bypass door motion is commanded as a function of sensed sideslip, which lags true sideslip. The sensed sideslip can be approximated analytically as the sum of a true sideslip component and a yaw rate component. Therefore the effect of the bypass doors can be accounted for in the sideslip and yaw rate derivatives as follows:

$$\beta_{lagged} = \beta + (K1)r$$

The yaw coefficient component of interest is $C_{n_\beta}\beta + C_{n_r}r + C_{n_{\delta_{bpd}}}\delta_{bpd}$ where δ_{bpd} equals $(K2)\beta_{lagged}$ or $(K2)[\beta + (K1)r]$. Substituting, the yaw coefficient component becomes $C_{n_\beta}\beta + C_{n_r}r + C_{n_{\delta_{bpd}}}[(K2)\beta + (K1)(K2)r]$ or $\left[C_{n_\beta} + C_{n_{\delta_{bpd}}}(K2)\right]\beta + \left[C_{n_r} + C_{n_{\delta_{bpd}}}(K1)(K2)\right]r$. The first term in the last expression is the effective C_{n_β}, and the second term is the effective C_{n_r}.

The first step in the analysis technique used to determine the bypass door derivatives was to fair preliminary derivatives, which were determined without a priori information. The second step was to rematch the maneuvers with an a priori weighting on the faired values of the bypass door derivatives (ref. 8). After rematching, the consistency of C_{n_β} and C_{n_r}, and, of course, the bypass door derivatives, was much improved. Only the derivatives obtained using a priori weighting for the bypass door derivatives are presented in this report.

When bypass door motion is used as an additional forcing function in the derivative analysis (that is, when bypass door derivatives are determined), the resulting sideslip and yaw rate derivatives should be the same as the derivatives obtained from the analysis of maneuvers made with the bypass doors fixed. The good agreement between the C_{n_β} values determined for the automatic inlets case by using the bypass doors as a variable and the C_{n_β} values determined for the fixed inlets case (fig. 7(a)) supports the automatic inlets analysis technique.

APPENDIX — Concluded

An example of the nonuniqueness of C_{n_β} and $C_{n_{\delta_{bpd}}}$ is presented in figure 11. The variation of C_{n_β} versus $C_{n_{\delta_{bpd}}}$ as a function of a priori weighting on $C_{n_{\delta_{bpd}}}$ was determined for three maneuver pairs. The variation is linear, as would be expected, and the ratio $C_{n_\beta}/C_{n_{\delta_{bpd}}}$ (approximately a constant for the conditions tested) represents the percentage of bypass door motion commanded per degree of sideslip. The ratio $C_{n_\beta}/C_{n_{\delta_{bpd}}}$ agrees well with $\Delta\delta_{bpd}/\Delta\beta$ measurements taken from flight data. The variation of C_{n_r} with $C_{n_{\delta_{bpd}}}$ is similar to the trend in figure 11 but is not as consistent.

REFERENCES

1. Schweikhard, W. G.; Gilyard, G. B.; Talbot, J. E.; and Brown, T. W.: Effects of Atmospheric Conditions on the Operating Characteristics of Supersonic Cruise Aircraft. IAF Paper 76-112, Internat. Astronaut. Federation, Oct. 1976.

2. Burcham, Frank W., Jr.; Montoya, Earl J.; and Lutschg, Phillip J.: Description of YF-12C Airplane, Propulsion System, and Instrumentation for Propulsion Research Flight Tests. NASA TM X-3099, 1974.

3. Gilyard, Glenn B.; Berry, Donald T.; and Belte, Daumants: Analysis of a Lateral-Directional Airframe/Propulsion System Interaction. NASA TM X-2829, 1973.

4. Gilyard, Glenn B.; and Smith, John W.: Results From Flight and Simulator Studies of a Mach 3 Cruise Longitudinal Autopilot. NASA TP-1180, 1978.

5. Lamb, Milton; Stallings, Robert L., Jr.; and Richardson, Celia S.: Aerodynamic Characteristics of 1/25-Scale Model of YF-12 Airplane at Mach 1.80 to 2.96 With and Without External Instrument Packages and Flow-Field Surveys at Mach 2.96. NASA TM X-2524, 1972.

6. Berry, Donald T.; and Gilyard, Glenn B.: Airframe/Propulsion System Interactions—An Important Factor in Supersonic Aircraft Flight Control. AIAA Paper 73-831, Aug. 1973.

7. Gilyard, Glenn B.; and Belte, Daumants: Flight-Determined Lag of Angle-of-Attack and Angle-of-Sideslip Sensors in the YF-12A Airplane From Analysis of Dynamic Maneuvers. NASA TN D-7819, 1974.

8. Maine, Richard E.; and Iliff, Kenneth W.: A FORTRAN Program for Determining Aircraft Stability and Control Derivatives From Flight Data. NASA TN D-7831, 1975.

9. Powers, Bruce G.: Phugoid Characteristics of a YF-12 Airplane With Variable Geometry Inlets Obtained in Flight Tests Near a Mach Number of 2.9. NASA TP-1107, 1977.

10. Yanagidate, Craig: Tuft Study of the Local Flow Around the Nacelle of the YF-12A Airplane. NASA TM X-56035, 1975.

11. Bailey, Rodney O.; Petroff, Daniel N.; and Shibata, Harry H.: Effect of Inlet-Airframe Interactions at High Mach Numbers on Aircraft Static-Stability and Control Effectiveness. NASA TM X-62,467, 1977.

TABLE 1.—LONGITUDINAL MANEUVER FLIGHT CONDITIONS

[Ventral on, camera pods on, S = 149.1 m (1605 ft), $\bar{c}$ = 11.5 m (37.7 ft)]

M	h_p, m (ft)	KEAS	W, kg (lb)	Center of gravity, percent $\bar{c}$	α_{trim}, deg	$\delta_{e_{trim}}$, deg	I_Y, kg-m^2 (slug-ft^2)
0.698	2,410 (7,900)	399	0.378×10^5 (0.834×10^5)	19.1	2.5	-2.6	1.649×10^6 (1.216×10^6)
0.814	4,570 (15,000)	404	0.530 (1.169)	20.3	3.2	-2.4	2.081 (1.535)
0.898	6,310 (20,700)	397	0.521 (1.149)	21.6	3.2	-2.8	2.020 (1.490)
0.944	7,130 (23,400)	394	0.514 (1.134)	22.1	3.3	-2.9	1.979 (1.460)
1.108	9,390 (30,800)	393	0.385 (0.849)	24.1	2.1	-4.6	1.658 (1.223)
1.218	10,300 (33,800)	403	0.386 (0.852)	24.3	2.1	-5.2	1.661 (1.225)
1.402	12,620 (41,400)	387	0.381 (0.839)	23.5	2.5	-6.3	1.653 (1.219)
1.602	14,080 (46,200)	393	0.383 (0.844)	24.7	2.9	-6.2	1.654 (1.220)
2.041	16,700 (54,800)	408	0.501 (1.104)	25.2	4.4	-7.0	1.905 (1.405)
2.196	17,830 (58,500)	402	0.474 (1.044)	27.1	4.3	-5.6	1.790 (1.320)
2.407	19,110 (62,700)	399	0.453 (0.999)	27.0	4.2	-6.2	1.735 (1.280)
2.591	20,330 (66,700)	390	0.414 (0.912)	26.0	4.2	-7.1	1.681 (1.240)
2.783	21,030 (69,000)	397	0.432 (0.952)	26.2	4.4	-6.8	1.699 (1.253)
2.910	21,520 (70,600)	399	0.388 (0.855)	26.2	3.9	-6.7	1.661 (1.225)
2.985	21,880 (71,800)	398	0.385 (0.849)	26.9	3.9	-6.1	1.674 (1.235)

TABLE 2.—LATERAL-DIRECTIONAL MANEUVER FLIGHT CONDITIONS

[S = 149.1 m (1605 ft), b = 17.3 m (56.7 ft), $I_X = 2.87 \times 10^5$ kg-m^2 (2.12×10^5 slug-ft^2)]

(a) Coldwall off

Ventral	M	h_p, m (ft)	KEAS	W, kg (lb)	Center of gravity, percent $\bar{c}$	α_{trim}, deg	$\delta_{e_{trim}}$, deg	I_Z, kg-m^2 (slug-ft^2)	I_{XZ}, kg-m^2 (slug-ft^2)
Off	0.699	2,500 (8,200)	397	0.345×10^5 (0.760×10^5)	18.7	2.2	-2.4	1.898×10^6 (1.400×10^6)	6.85×10^4 (5.05×10^4)
	0.800	4,790 (15,700)	392	0.340 (0.750)	20.2	2.3	-2.5	1.885 (1.390)	6.89 (5.08)
	0.891	6,100 (20,000)	400	0.345 (0.760)	20.8	2.1	-2.8	1.898 (1.400)	6.85 (5.05)
	0.926	6,800 (22,300)	396	0.349 (0.770)	21.2	2.2	-3.0	1.905 (1.405)	6.83 (5.04)
	1.085	9,270 (30,400)	388	0.354 (0.780)	26.6	2.1	-2.6	1.912 (1.410)	6.85 (5.05)
	1.205	10,270 (33,700)	400	0.363 (0.800)	26.8	1.9	-3.5	1.925 (1.420)	6.82 (5.03)
	1.410	12,160 (39,900)	403	0.372 (0.820)	26.6	2.2	-4.7	1.939 (1.430)	6.82 (5.03)
	1.636	13,900 (45,600)	408	0.422 (0.930)	25.9	3.2	-5.8	1.997 (1.473)	6.96 (5.13)
	2.000	16,610 (54,500)	403	0.404 (0.890)	25.7	3.6	-5.8	1.979 (1.460)	6.91 (5.10)
	2.211	17,830 (58,500)	405	0.376 (0.830)	26.1	3.4	-5.4	1.952 (1.440)	6.82 (5.03)
	2.384*	18,990 (62,300)	399	0.449 (0.990)	26.9	4.3	-6.3	2.034 (1.500)	7.05 (5.20)
	2.395	18,960 (62,200)	401	0.458 (1.010)	26.9	4.3	-6.0	2.047 (1.510)	7.12 (5.25)
	2.484*	19,900 (65,300)	387	0.397 (0.875)	26.2	3.8	-6.5	1.973 (1.455)	6.91 (5.10)
	2.586	20,150 (66,100)	395	0.420 (0.925)	26.5	4.2	-6.6	1.997 (1.473)	6.96 (5.13)
	2.599	20,090 (65,900)	399	0.472 (1.040)	27.0	4.6	-6.0	2.088 (1.540)	7.12 (5.25)
	2.700*	20,570 (67,500)	399	0.374 (0.825)	25.1	3.7	-7.7	1.946 (1.435)	6.83 (5.04)
	2.807	21,370 (70,100)	390	0.399 (0.880)	26.3	4.1	-6.6	1.979 (1.460)	6.89 (5.08)
	2.813	20,880 (68,500)	406	0.370 (0.815)	24.7	3.6	-7.5	1.939 (1.430)	6.82 (5.03)
On	0.704	2,190 (7,200)	407	0.535 (1.179)	22.5	3.3	-2.1	2.413 (1.780)	6.37 (4.70)
	0.800	4,390 (14,400)	402	0.512 (1.129)	22.0	3.2	-2.4	2.264 (1.670)	6.91 (5.10)
	0.896	6,000 (19,700)	405	0.494 (1.089)	21.8	3.0	-2.9	2.169 (1.600)	7.05 (5.20)
	0.932	6,520 (21,400)	406	0.468 (1.032)	20.9	2.8	-3.2	2.074 (1.530)	7.05 (5.20)
	1.222	10,420 (34,200)	400	0.430 (0.947)	23.1	2.6	-5.3	2.007 (1.480)	6.91 (5.10)
	1.417	12,160 (39,900)	405	0.491 (1.082)	26.2	3.2	-6.1	2.156 (1.590)	7.05 (5.20)
	1.638	13,990 (45,900)	405	0.477 (1.052)	27.0	3.6	-5.2	2.102 (1.550)	7.19 (5.30)
	1.838	15,390 (50,500)	408	0.445 (0.982)	26.4	3.7	-5.9	2.034 (1.500)	7.05 (5.20)
	2.001	16,790 (55,100)	398	0.489 (1.077)	25.0	4.3	-6.6	2.156 (1.590)	7.05 (5.20)
	2.197	17,830 (58,500)	402	0.469 (1.034)	27.0	4.1	-5.7	2.074 (1.530)	7.19 (5.30)
	2.415	19,140 (62,800)	399	0.445 (0.981)	27.0	4.0	-6.2	2.034 (1.500)	7.05 (5.20)
	2.619	20,270 (66,500)	397	0.407 (0.897)	25.8	4.0	-6.7	1.979 (1.460)	6.91 (5.10)
	2.779	20,850 (68,400)	402	0.429 (0.946)	26.2	4.4	-7.0	2.007 (1.480)	6.91 (5.10)
	2.910	21,580 (70,800)	398	0.380 (0.838)	26.2	3.7	-6.5	1.952 (1.440)	6.91 (5.10)
	3.000	21,820 (71,600)	401	0.381 (0.841)	26.8	3.8	-5.9	1.952 (1.440)	6.91 (5.10)

*Fixed bypass doors.

TABLE 2.—Concluded

(b) Coldwall on

Ventral	M	h_p, m (ft)	KEAS	W, kg (lb)	Center of gravity, percent $\bar{c}$	α_{trim}, deg	$\delta_{e_{trim}}$, deg	I_Z, kg-m^2 (slug-ft^2)	I_{XZ}, kg-m^2 (slug-ft^2)
Off	0.904	6,000 (19,700)	408	0.508 × 10^5 (1.120 × 10^5)	22.0	3.0	-2.7	2.237 × 10^6 (1.650 × 10^6)	6.91 × 10^4 (5.10 × 10^4)
	0.925	6,400 (21,000)	406	0.503 (1.110)	22.9	3.0	-2.7	2.190 (1.615)	7.05 (5.20)
	1.219	10,330 (33,900)	402	0.458 (1.010)	23.1	2.8	-6.0	2.051 (1.513)	7.12 (5.25)
	1.621	14,020 (46,000)	401	0.494 (1.090)	25.0	3.9	-6.5	2.169 (1.600)	7.05 (5.20)
	2.006	16,640 (54,600)	403	0.458 (1.010)	26.5	4.0	-5.3	2.051 (1.513)	7.12 (5.25)
	2.102	17,310 (56,800)	401	0.454 (1.000)	26.4	4.0	-5.3	2.068 (1.525)	7.09 (5.23)
	2.199	17,860 (58,600)	402	0.435 (0.960)	26.0	4.0	-5.5	2.013 (1.485)	7.02 (5.18)
	2.319	18,560 (60,900)	402	0.404 (0.890)	25.2	3.8	-5.7	1.979 (1.460)	6.91 (5.10)
	2.409	19,170 (62,900)	397	0.390 (0.860)	26.1	3.8	-5.6	1.966 (1.450)	6.89 (5.08)
Off	0.875*	6,130 (20,100)	391	0.517 (1.140)	22.2	3.3	-2.8	2.285 (1.685)	6.82 (5.03)
	0.927*	6,830 (22,400)	396	0.513 (1.130)	22.7	3.2	-3.1	2.257 (1.665)	6.89 (5.08)
	1.225*	10,450 (34,300)	400	0.472 (1.040)	25.9	3.0	-5.2	2.088 (1.540)	7.12 (5.25)
	1.624*	13,960 (45,800)	403	0.438 (0.965)	26.6	3.6	-6.0	2.017 (1.488)	7.05 (5.20)
	2.224*	17,830 (58,500)	407	0.458 (1.010)	26.5	4.1	-5.5	2.047 (1.510)	7.12 (5.25)
	2.308*	18,560 (60,900)	399	0.445 (0.980)	26.2	4.1	-5.9	2.027 (1.495)	7.05 (5.20)
	2.423	19,290 (63,300)	396	0.395 (0.870)	26.0	3.7	-5.8	1.970 (1.453)	6.89 (5.08)
On	2.015	16,980 (55,700)	394	0.463 (1.020)	27.9	4.0	-5.5	2.061 (1.520)	7.05 (5.20)
	2.222	17,740 (58,200)	410	0.446 (0.984)	27.7	3.7	-5.5	2.034 (1.500)	7.05 (5.20)
	2.373	18,900 (62,000)	399	0.429 (0.946)	27.5	3.9	-6.2	2.007 (1.480)	6.91 (5.10)
	2.488	19,390 (63,600)	404	0.420 (0.925)	27.4	3.8	-6.2	1.993 (1.470)	6.91 (5.10)
	2.603	20,270 (66,500)	394	0.389 (0.857)	26.8	3.6	-6.0	1.966 (1.450)	6.91 (5.10)
	2.702	20,630 (67,700)	397	0.380 (0.838)	27.0	3.6	-5.9	1.952 (1.440)	6.91 (5.10)
	2.786	21,000 (68,900)	399	0.370 (0.816)	27.2	3.5	-5.8	1.939 (1.430)	6.78 (5.00)
	2.925	21,490 (70,500)	403	0.358 (0.790)	27.6	3.4	-5.6	1.925 (1.420)	6.78 (5.00)
	3.000	21,520 (70,600)	411	0.436 (0.962)	26.6	4.3	-5.9	2.020 (1.490)	7.05 (5.20)
	3.000	21,490 (70,500)	412	0.393 (0.866)	25.1	3.8	-7.4	1.966 (1.450)	6.91 (5.10)

*Coldwall insulation on.

TABLE 3—FLIGHT CONDITIONS AT WHICH MANEUVERS ANALYZED FOR LOW SPEED LATERAL-DIRECTIONAL DERIVATIVES WERE INITIATED

[S = 149.1 m (1605 ft), b = 17.3 m (56.7 ft), I_X = 2.87 × 10^5 kg-m^2 (2.12 × 10^5 slug-ft^2)]

KEAS	M	h_p, m (ft)	W, kg (lb)	Center of gravity, percent $\bar{c}$	α_{trim}, deg	$\delta_{e_{trim}}$, deg	I_Z, kg-m^2 (slug-ft^2)	I_{XZ}, kg-m^2 (slug-ft^2)
293	0.696	7,010 (23,000)	0.517 × 10^5 (1.140 × 10^5)	21.0	5.3	-2.7	2.278 × 10^6 (1.680 × 10^6)	6.78 × 10^4 (5.00 × 10^4)
300	0.798	8,600 (28,200)	0.485 (1.070)	21.6	4.5	-2.7	2.129 (1.570)	7.05 (5.20)
300	0.895	10,120 (33,200)	0.463 (1.020)	20.9	4.5	-3.4	2.061 (1.520)	7.05 (5.20)
295	0.903	10,490 (34,400)	0.449 (0.990)	20.2	4.6	-3.8	2.034 (1.500)	7.05 (5.20)
294	0.921	10,760 (35,300)	0.435 (0.960)	19.8	4.3	-3.9	2.007 (1.480)	7.05 (5.20)
303	0.956	10,850 (35,600)	0.494 (1.090)	21.6	4.8	-3.3	2.169 (1.600)	6.37 (4.70)
349	0.705	4,630 (15,200)	0.526 (1.160)	21.3	4.2	-2.5	2.346 (1.730)	6.64 (4.90)
359	0.811	6,310 (20,700)	0.513 (1.130)	22.3	3.7	-2.3	2.264 (1.670)	6.91 (5.10)
350	0.904	8,170 (26,800)	0.381 (0.840)	21.0	2.7	-3.1	1.952 (1.440)	6.78 (5.00)
345	0.905	8,380 (27,500)	0.367 (0.810)	20.3	2.7	-3.2	1.939 (1.430)	6.78 (5.00)
349	0.929	8,600 (28,200)	0.363 (0.800)	19.9	2.7	-3.3	1.925 (1.420)	6.78 (5.00)
353	0.946	8,690 (28,500)	0.485 (1.070)	21.5	3.6	-2.9	2.142 (1.580)	7.05 (5.20)
407	0.704	2,190 (7,200)	0.535 (1.179)	22.5	3.3	-2.1	2.413 (1.780)	6.37 (4.70)
402	0.800	4,390 (14,400)	0.512 (1.129)	22.0	3.2	-2.4	2.264 (1.670)	6.91 (5.10)
405	0.896	6,000 (19,700)	0.494 (1.089)	21.8	3.0	-2.9	2.169 (1.600)	7.05 (5.20)
402	0.906	6,250 (20,500)	0.482 (1.062)	21.5	3.6	-3.0	2.115 (1.560)	7.19 (5.30)
406	0.932	6,520 (21,400)	0.468 (1.032)	20.9	2.8	-3.2	2.074 (1.530)	7.05 (5.20)

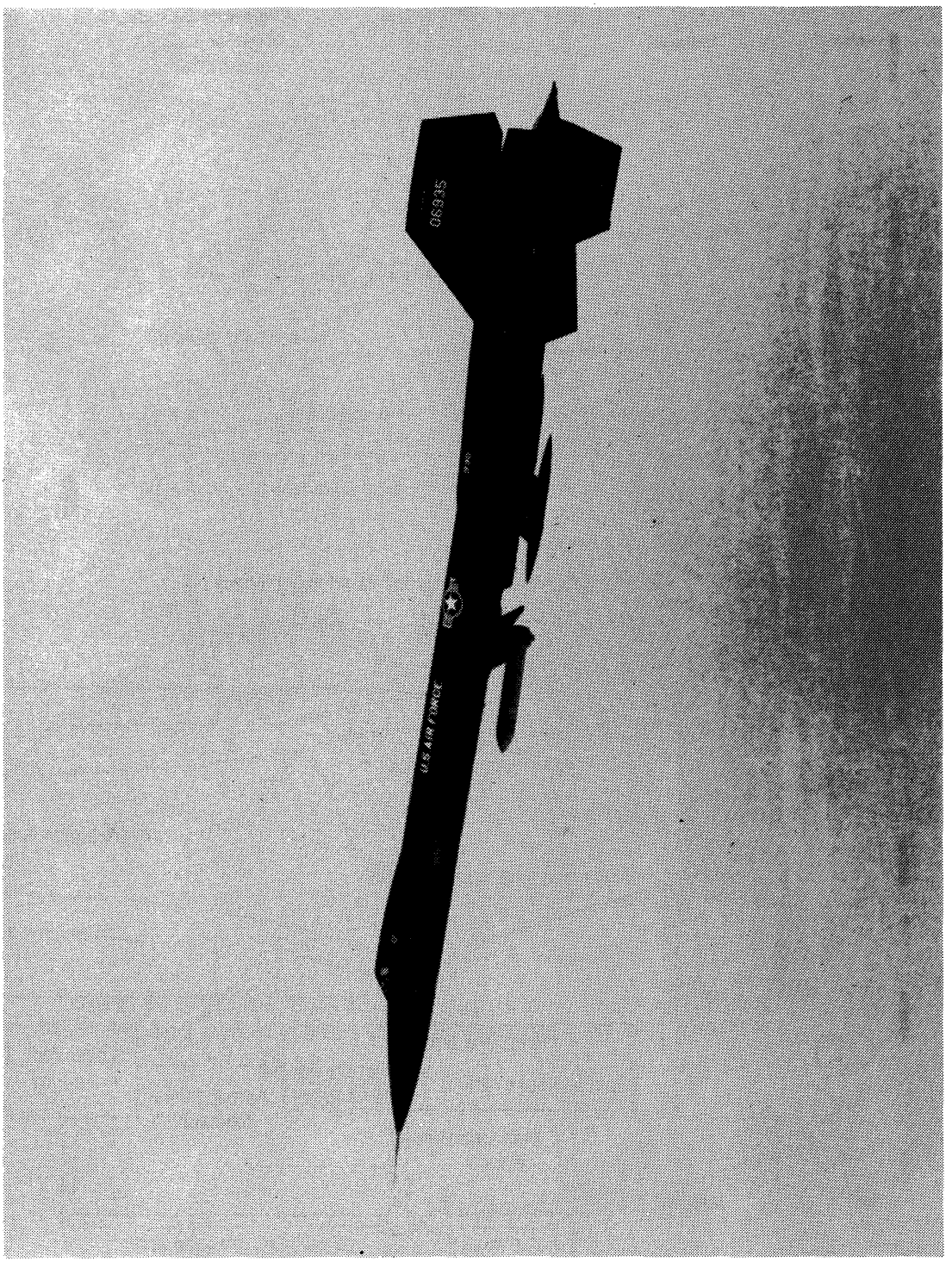

ECN 6993

Figure 1. Test airplane.

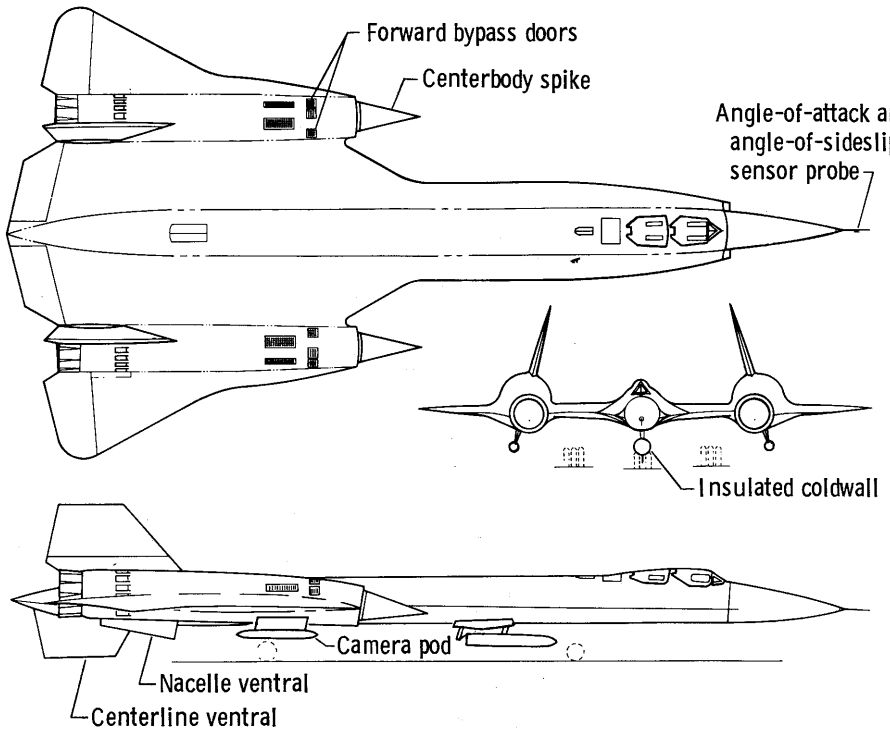

Figure 2. Three-view drawing of test airplane.

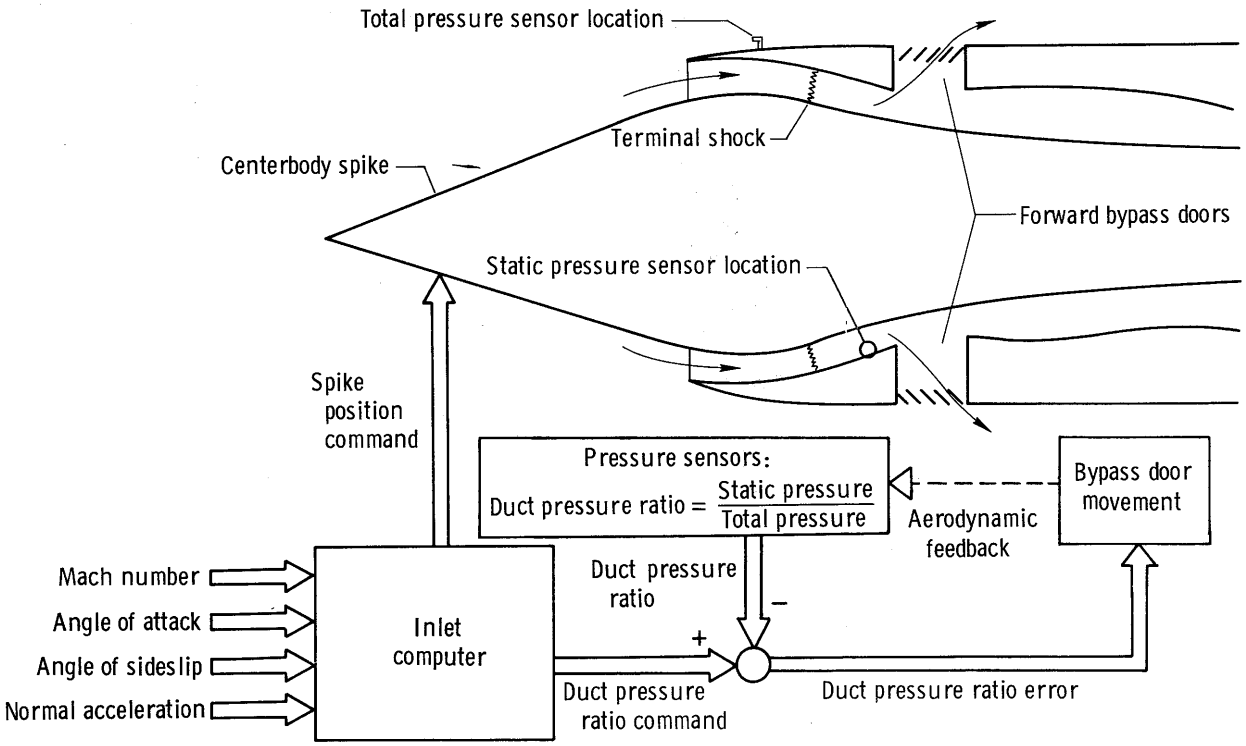

Figure 3. Inlet control system.

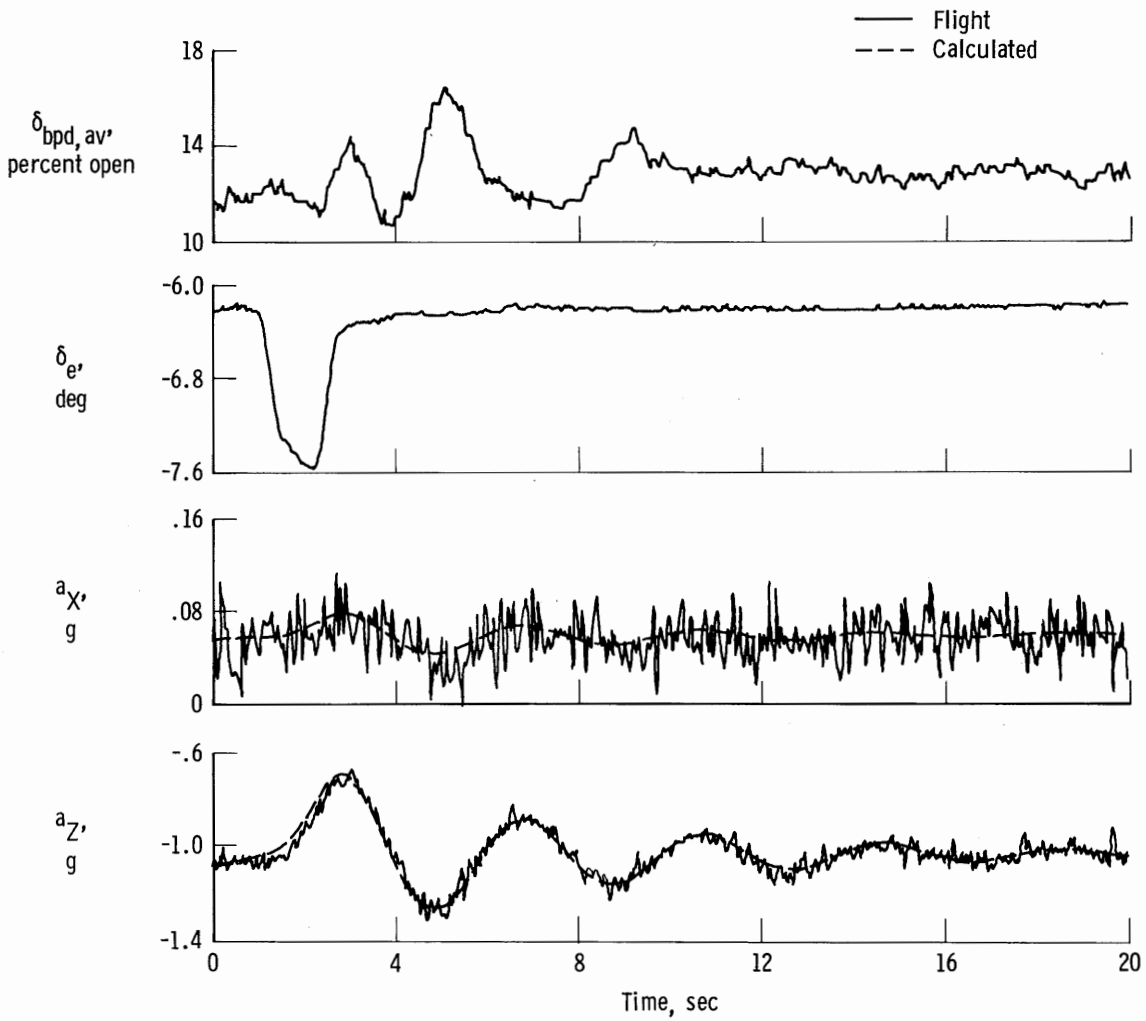

Figure 4. Typical match of pullup and release maneuver time history. Ventral and camera pods on; coldwall off; M = 2.985.

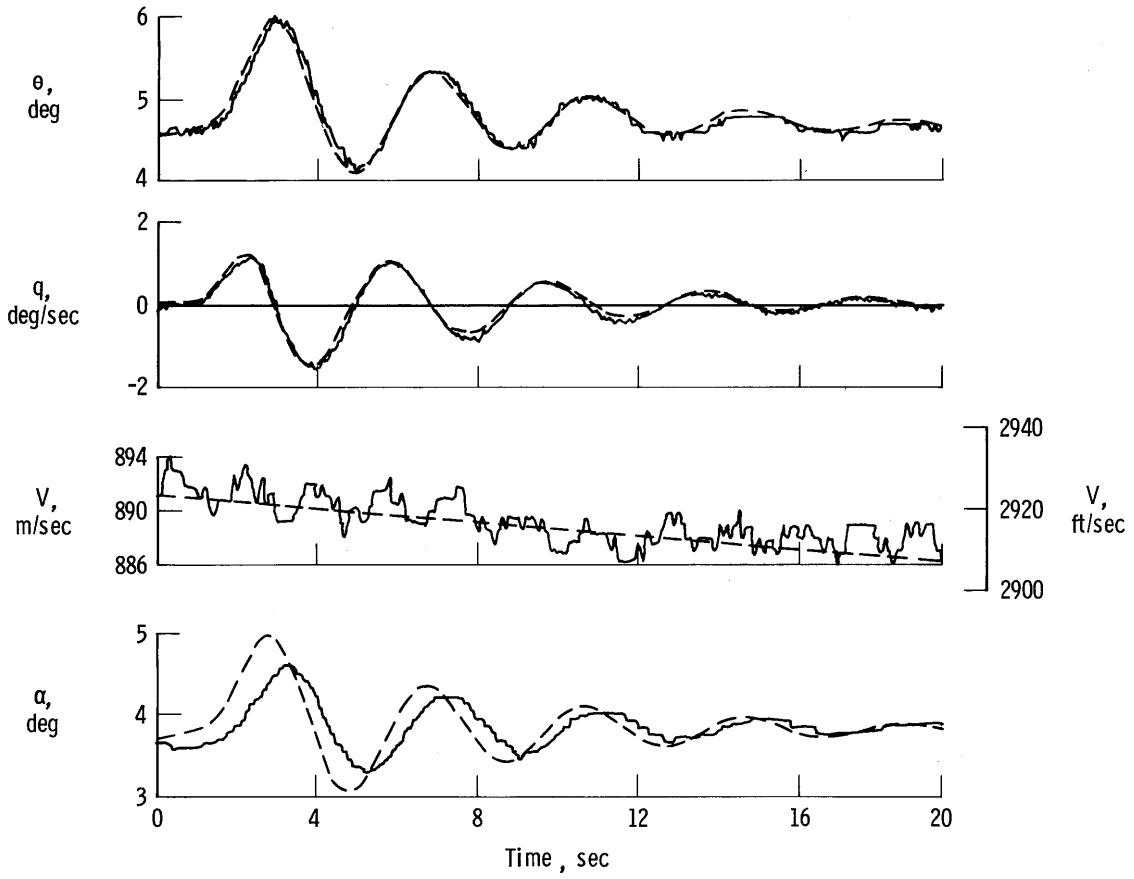

Figure 4. Concluded.

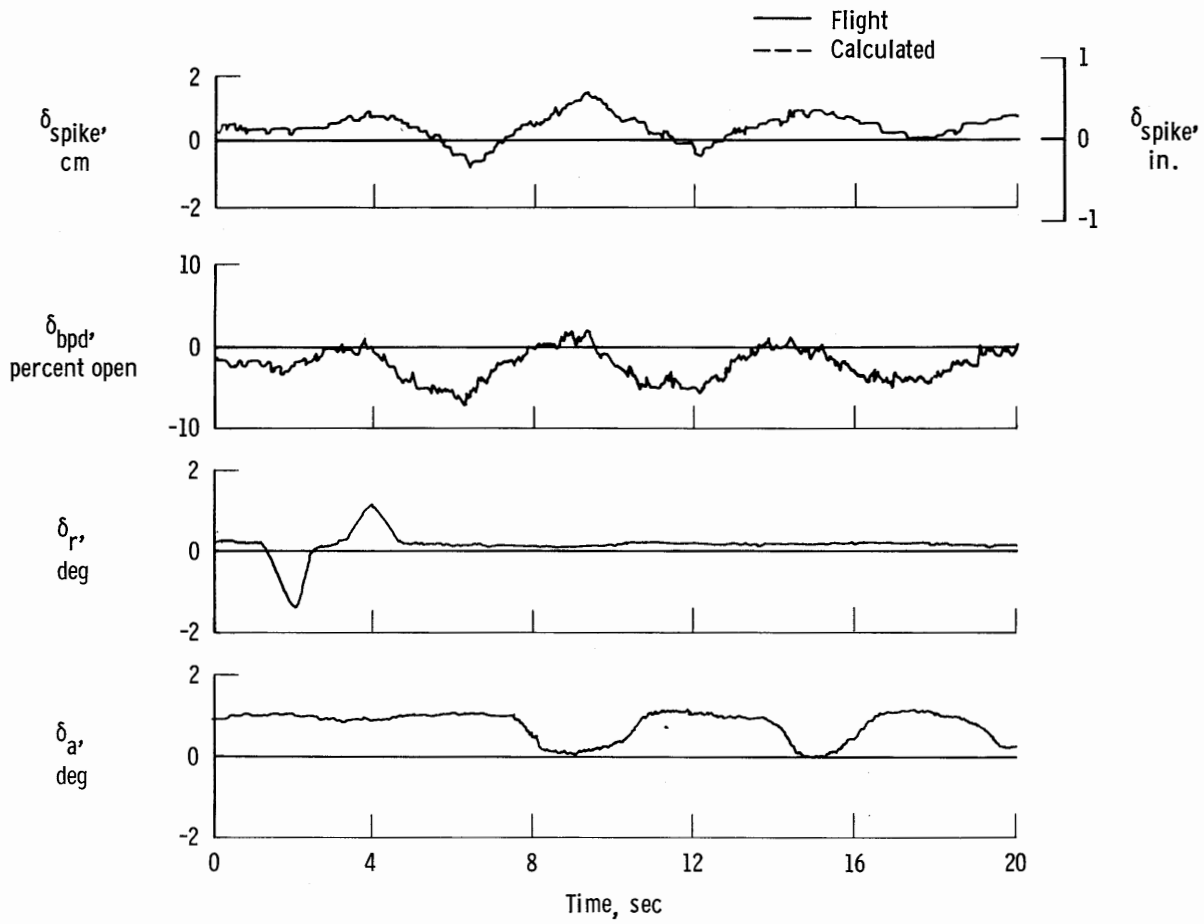

(a) Rudder doublet.

Figure 5. Typical match of rudder and aileron doublet maneuver time histories. Ventral, coldwall, and camera pods on; M = 3.000.

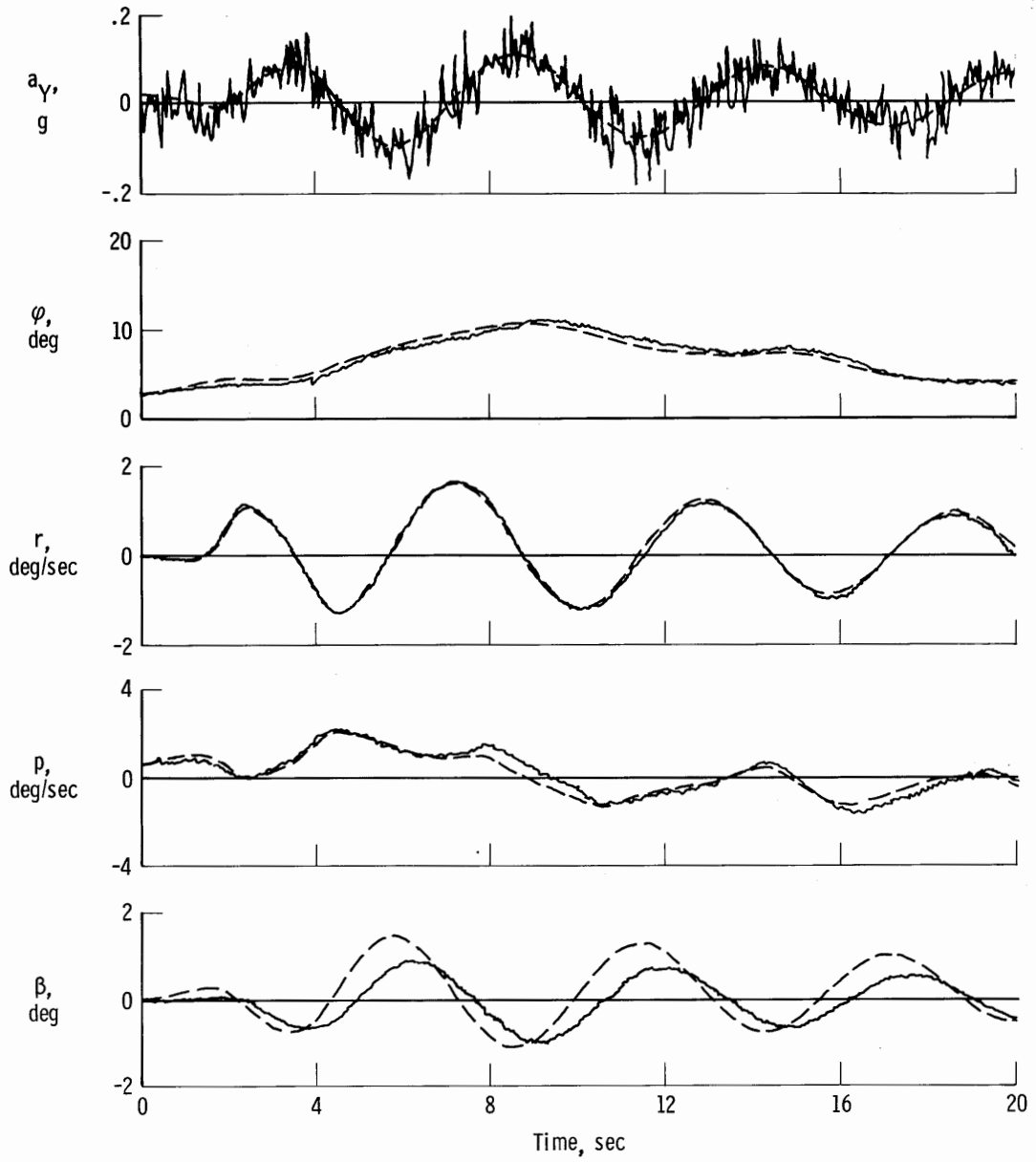

(a) Concluded.

Figure 5. Continued.

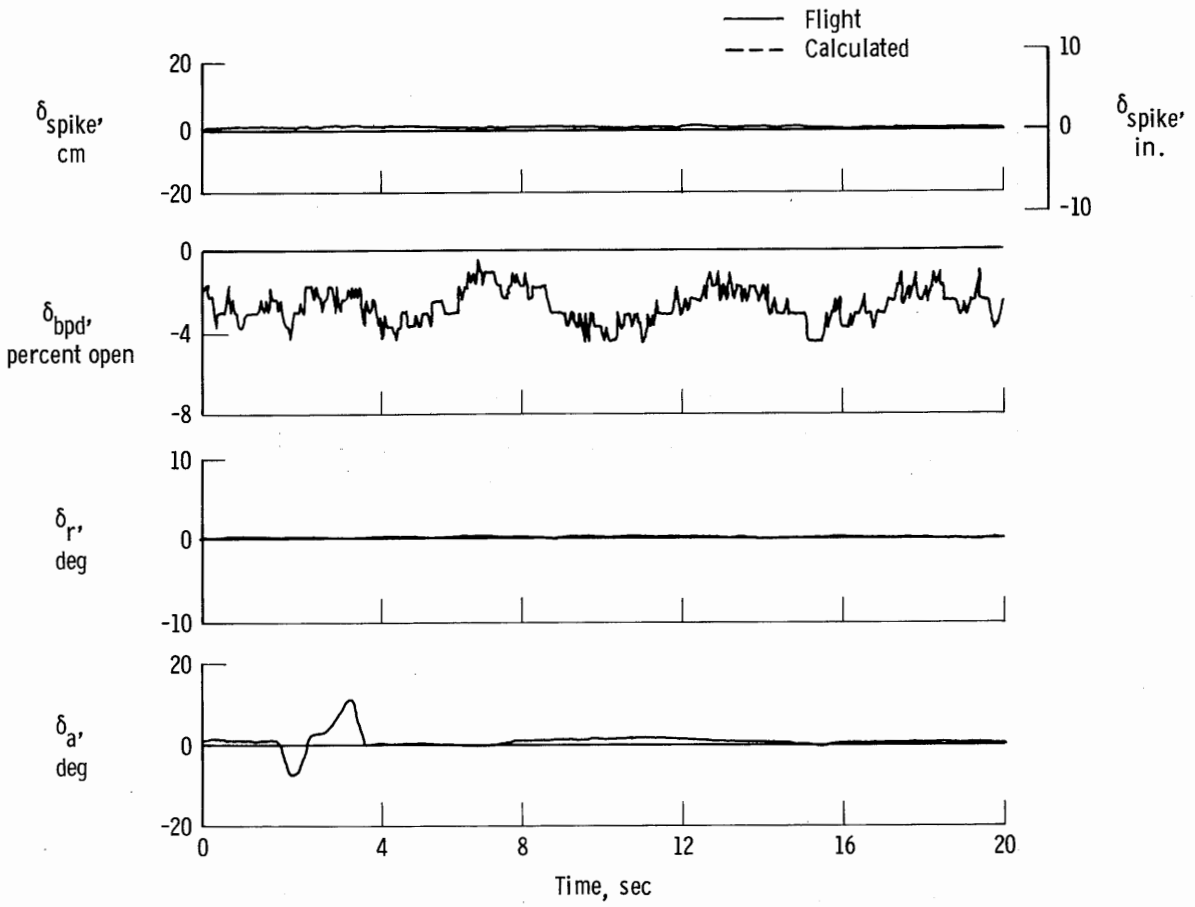

(b) Aileron doublet.

Figure 5. Continued.

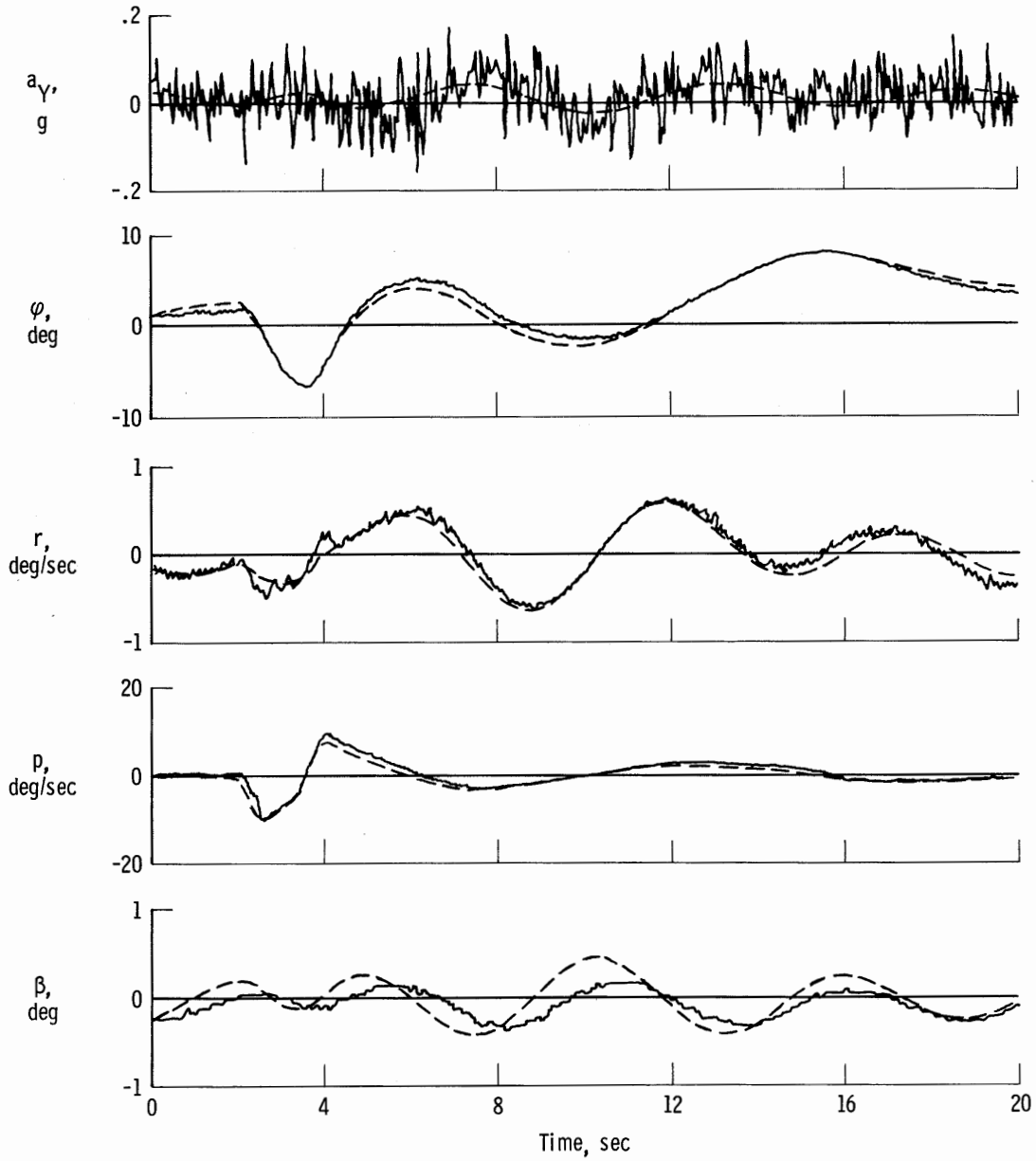

(b) Concluded.

Figure 5. Concluded.

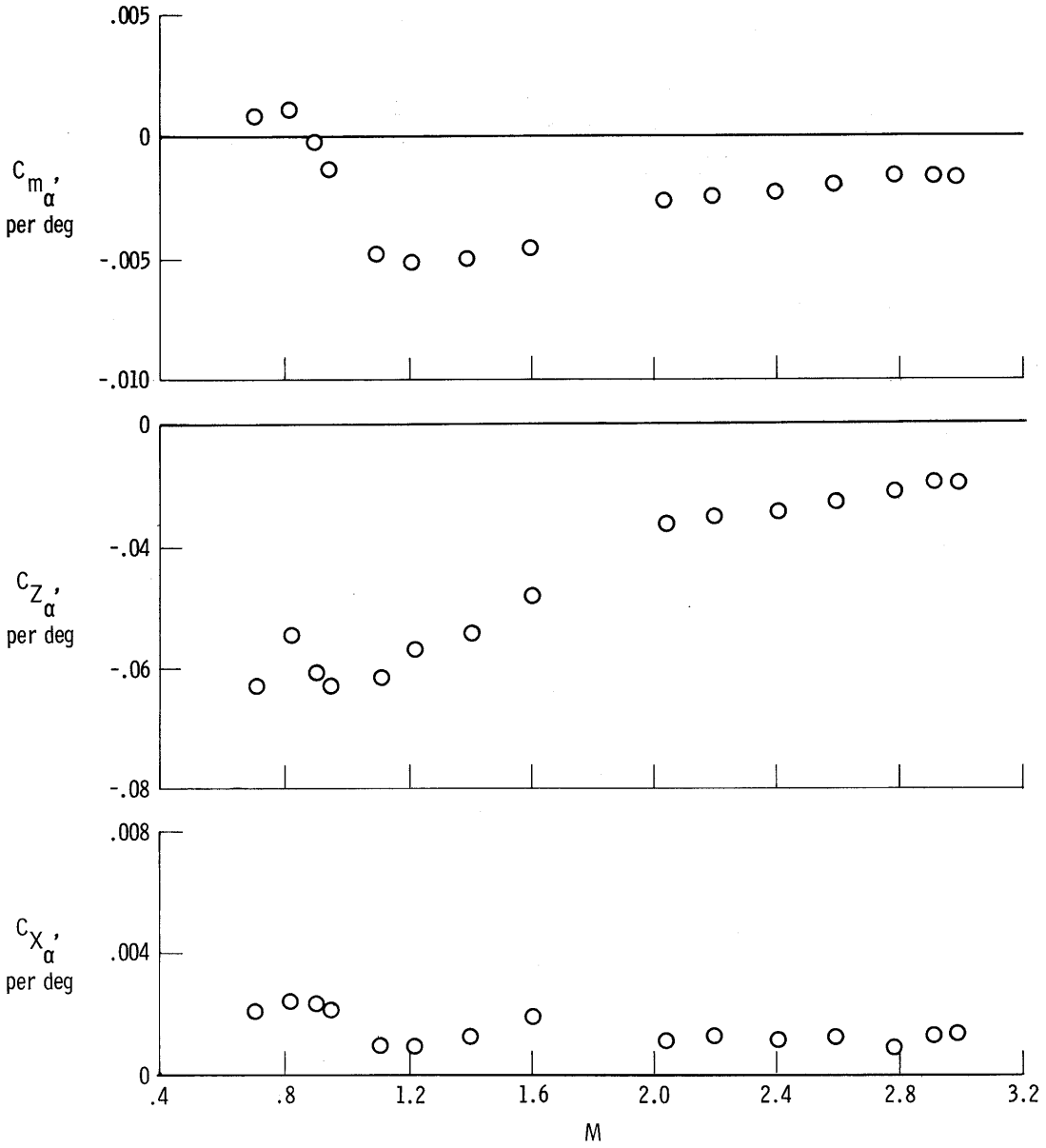

(a) C_{m_α}, C_{Z_α}, C_{X_α}.

Figure 6. Variation of longitudinal flight-determined derivatives with Mach number. Ventral on; coldwall off.

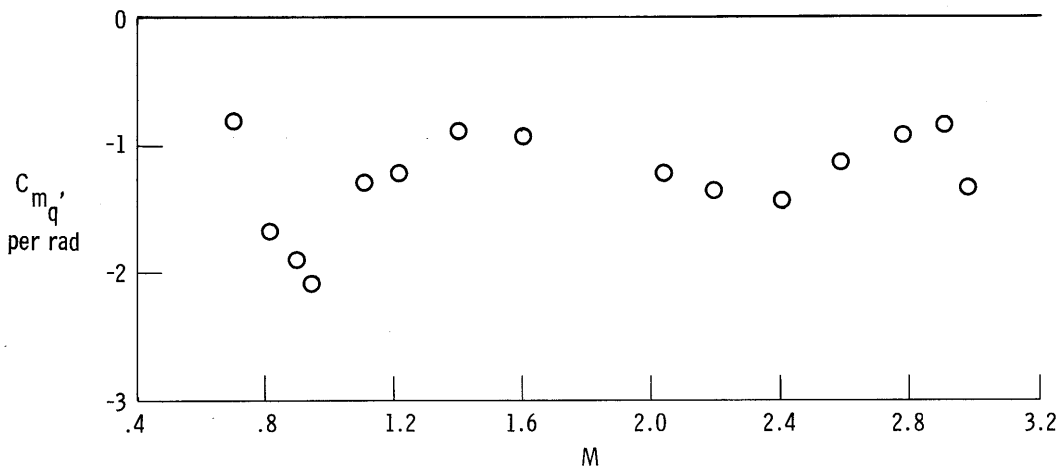

(b) C_{m_q}.

Figure 6. Continued.

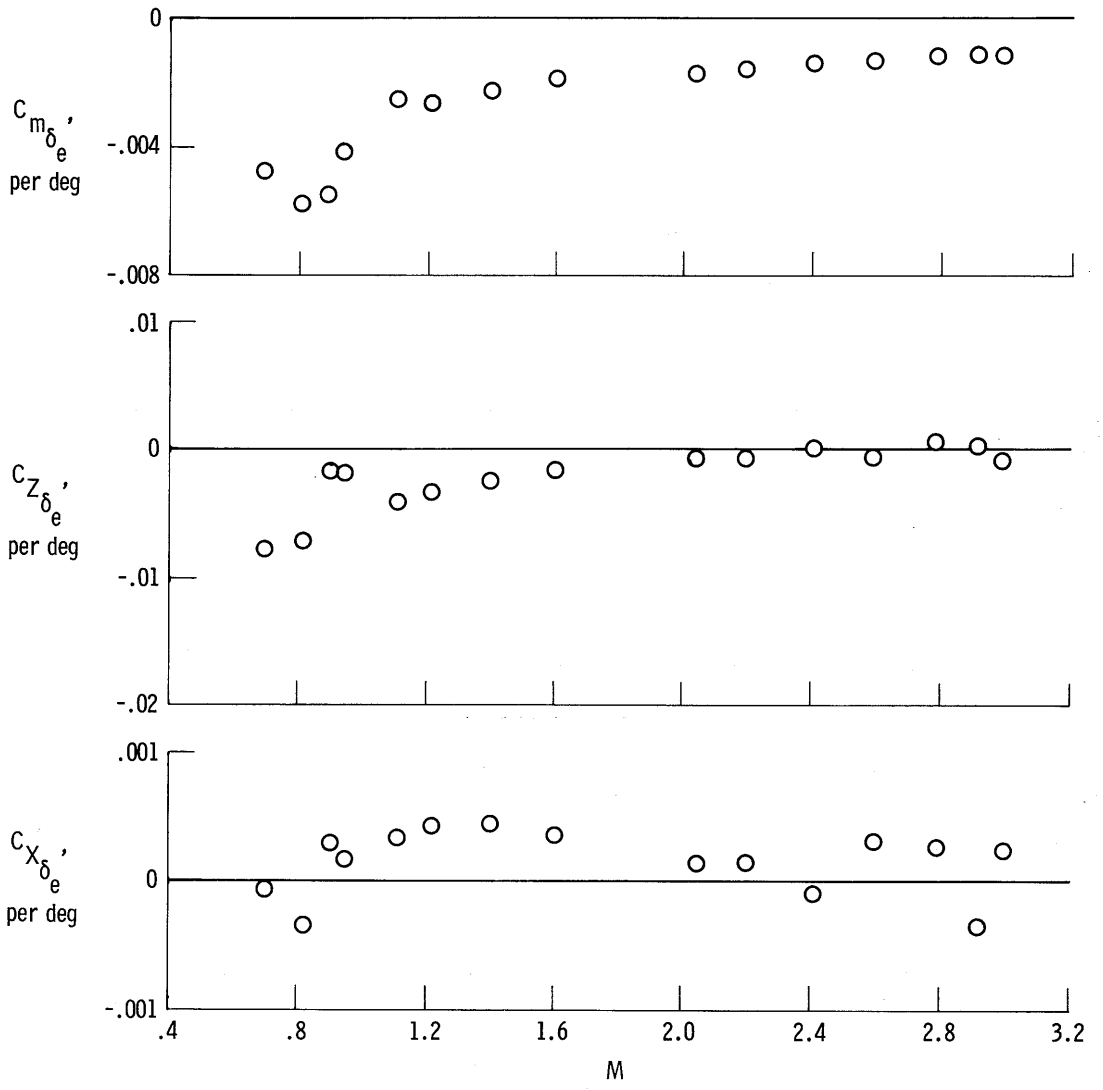

(c) $C_{m_{\delta_e}}$, $C_{Z_{\delta_e}}$, $C_{X_{\delta_e}}$.

Figure 6. Continued.

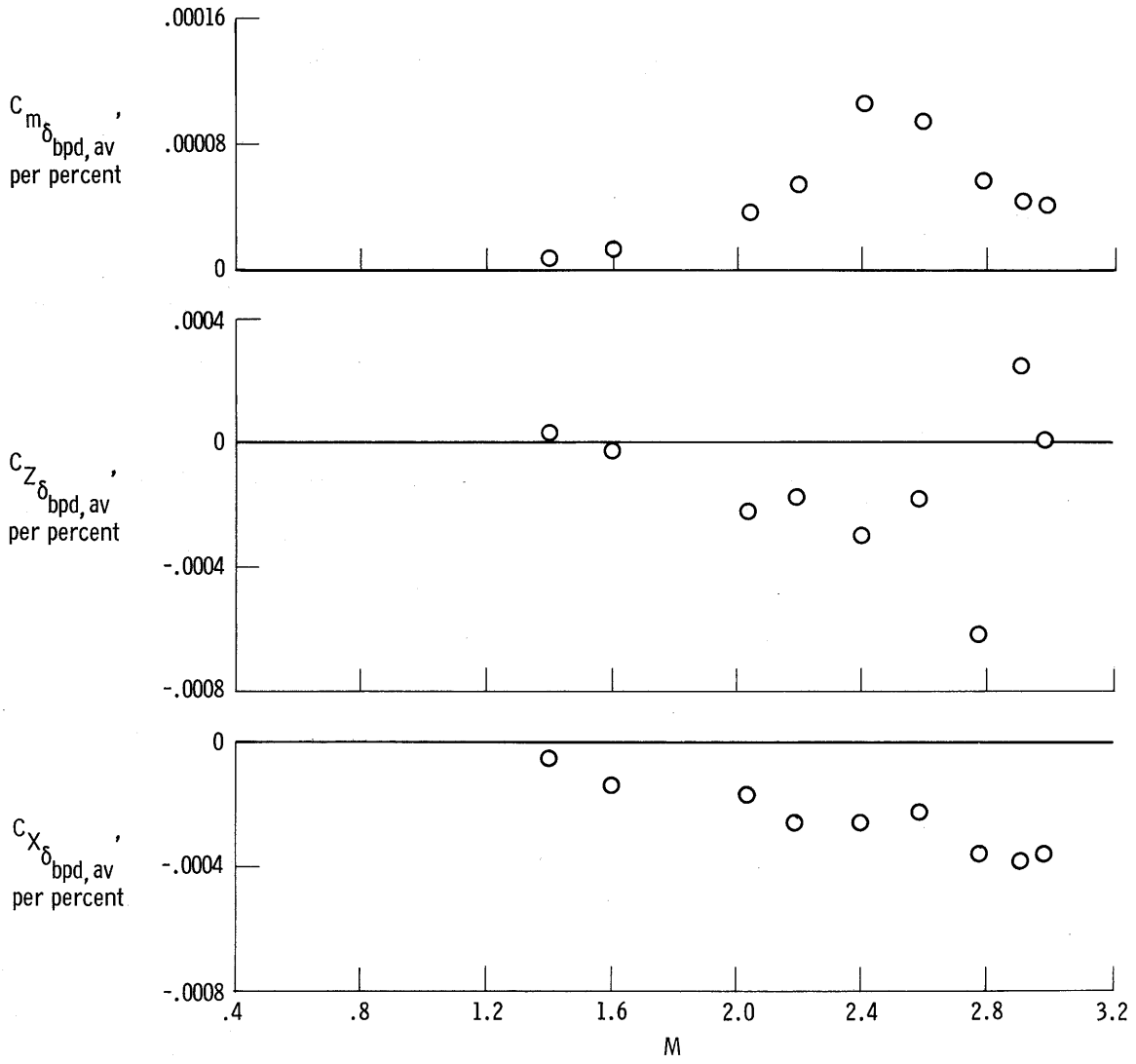

(d) $C_{m_{\delta_{bpd,\,av}}}$, $C_{Z_{\delta_{bpd,\,av}}}$, $C_{X_{\delta_{bpd,\,av}}}$.

Figure 6. Concluded.

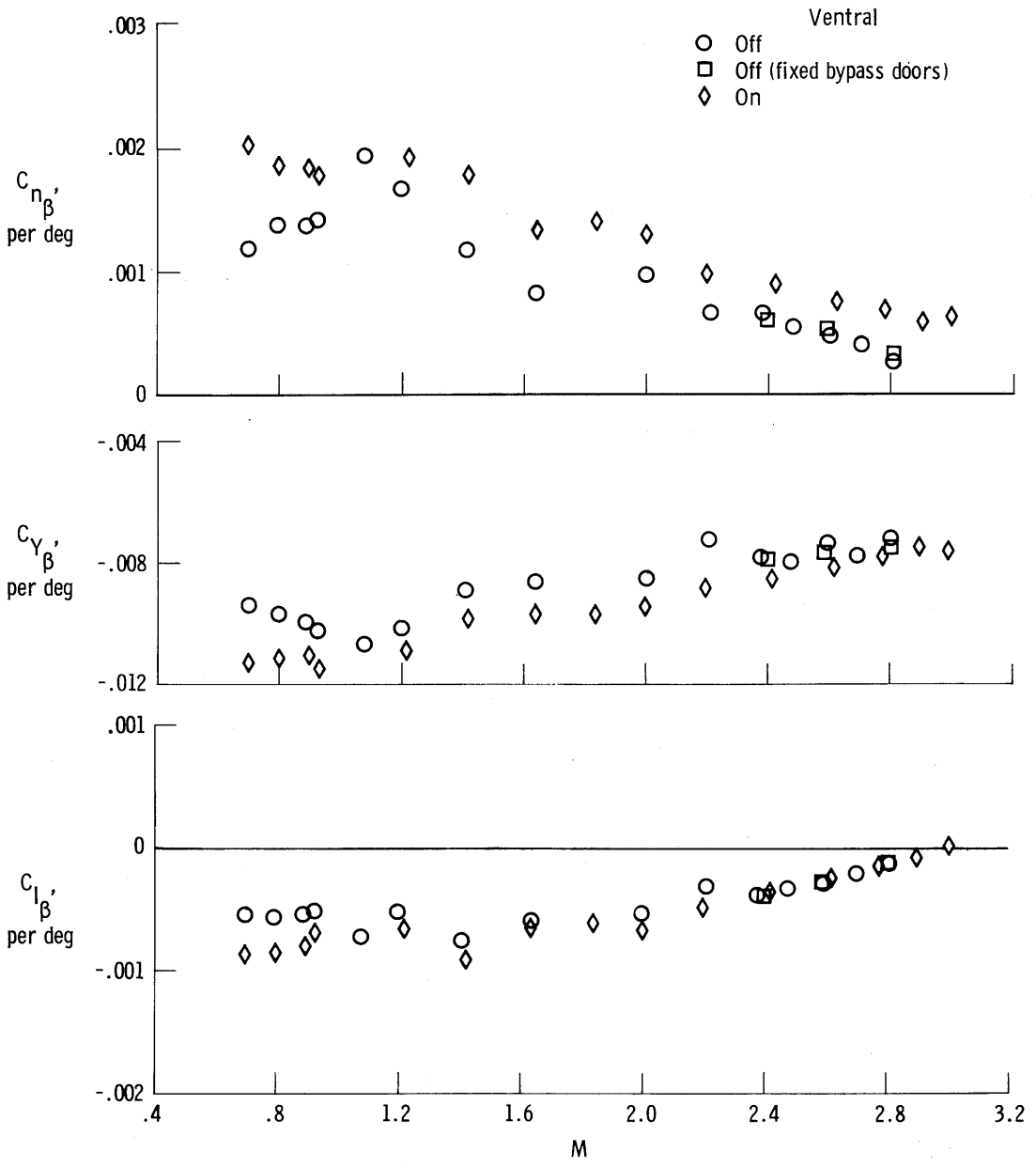

(a) C_{n_β}, C_{Y_β}, C_{l_β}.

Figure 7. Variation of coldwall-off lateral-directional derivatives with Mach number.

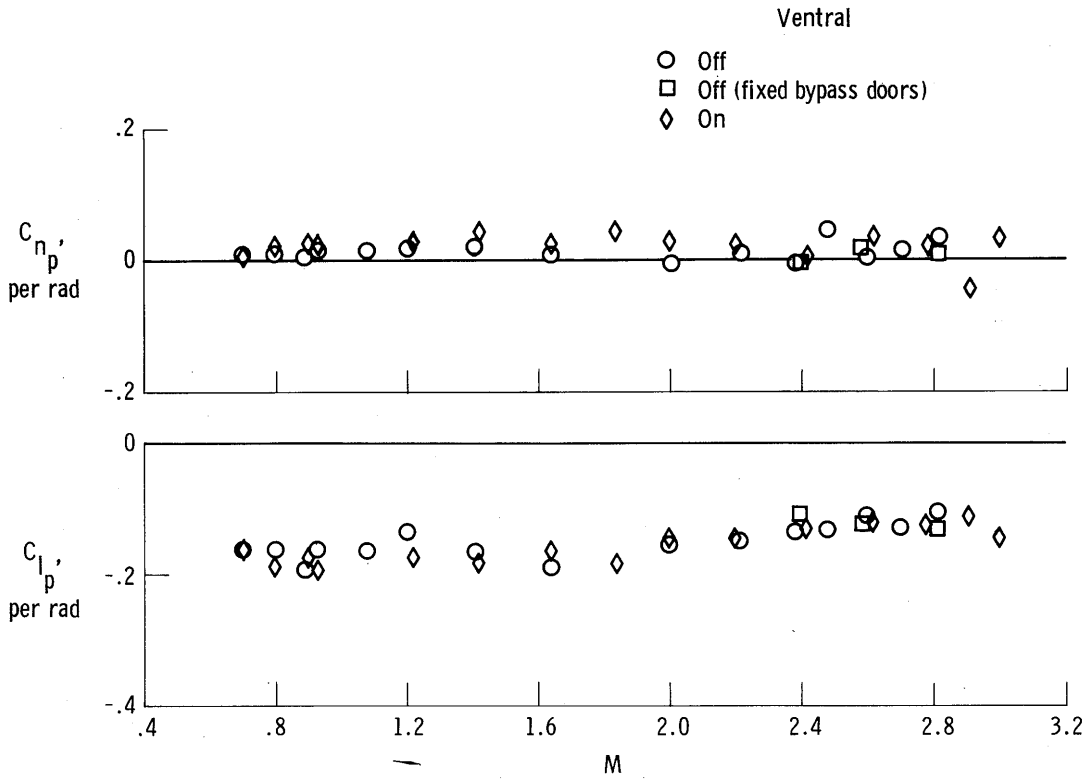

(b) C_{n_p}, C_{l_p}.

Figure 7. Continued.

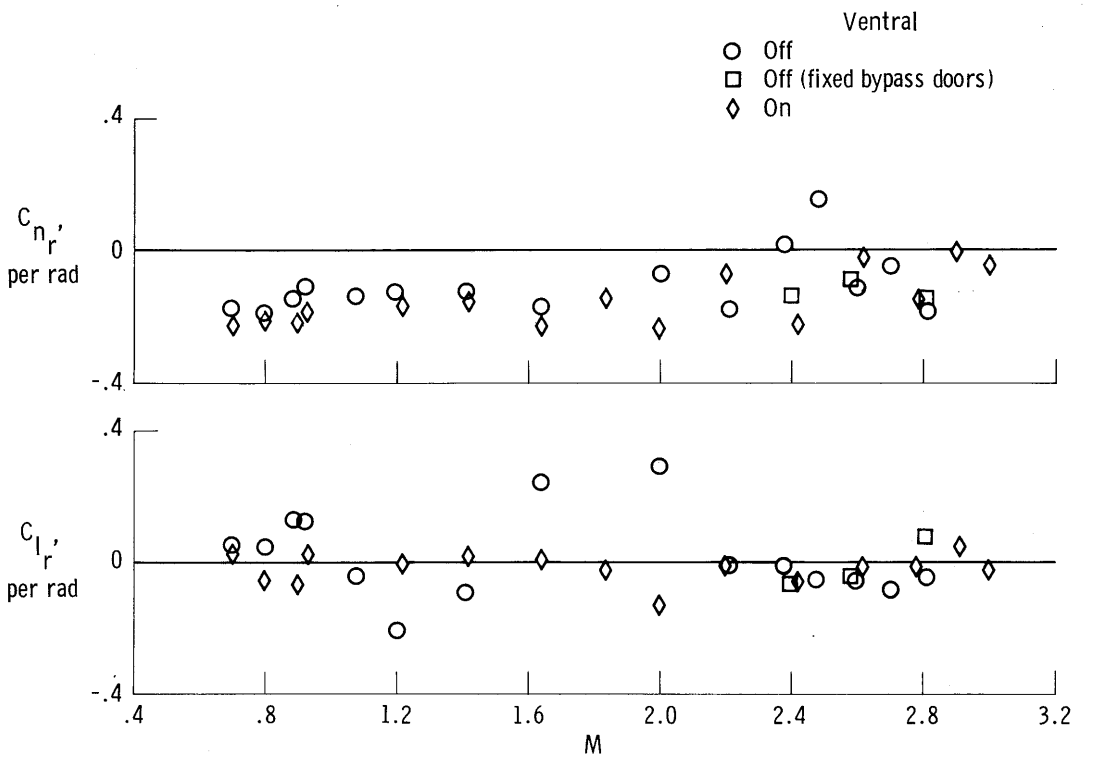

(c) C_{n_r}, C_{l_r}.

Figure 7. Continued.

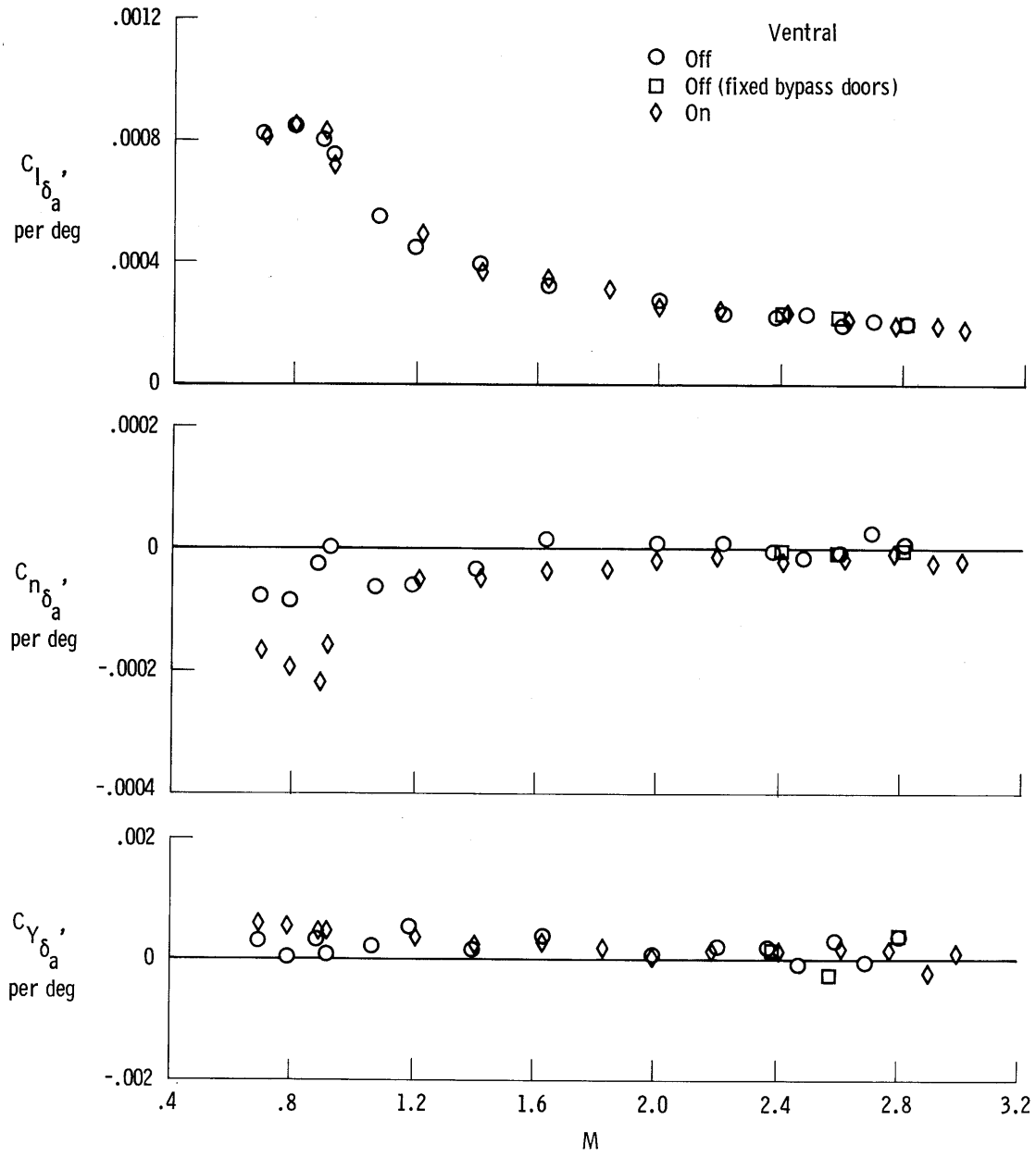

(d) $C_{l_{\delta_a}}$, $C_{n_{\delta_a}}$, $C_{Y_{\delta_a}}$.

Figure 7. Continued.

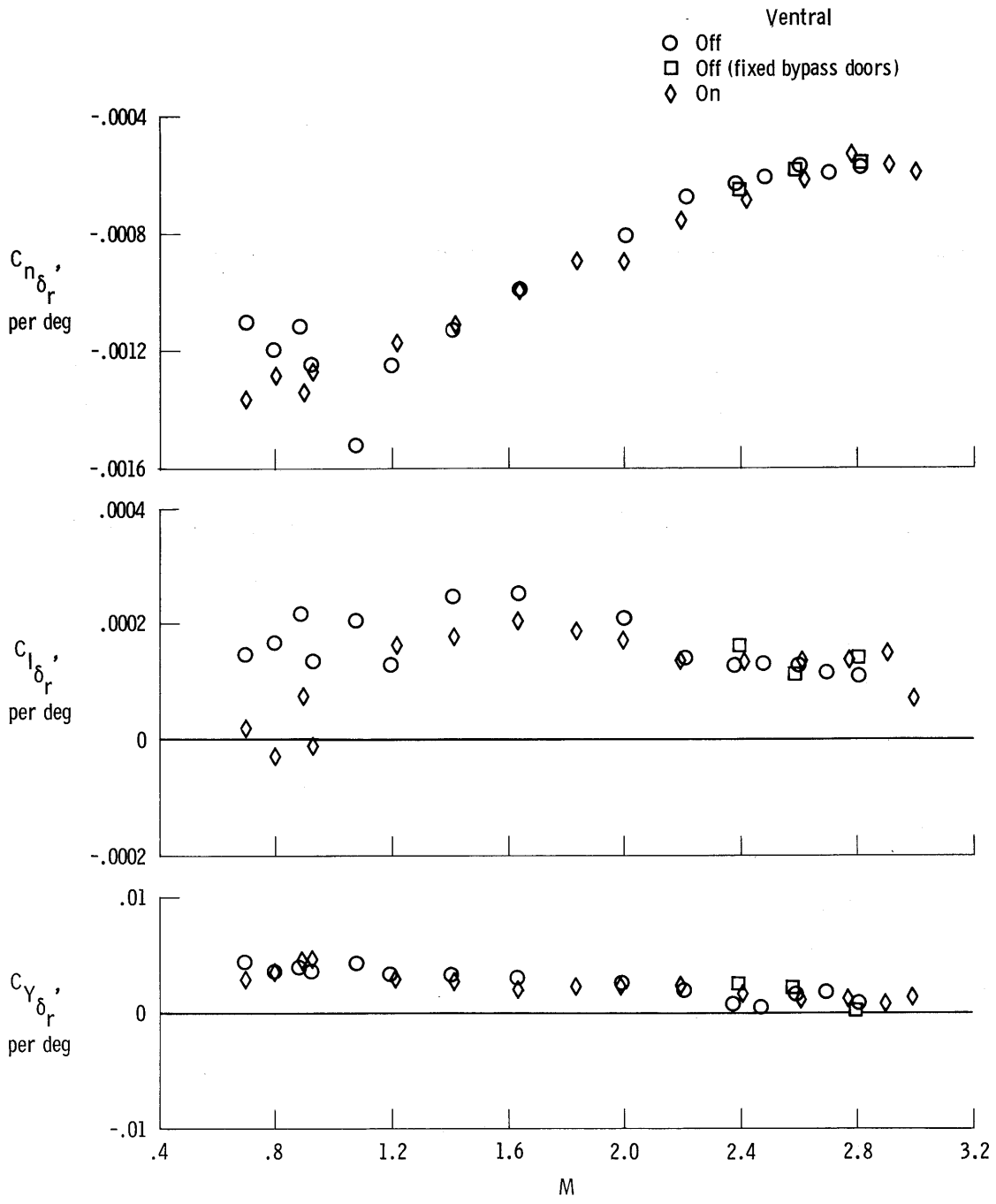

(e) $C_{n_{\delta_r}}$, $C_{l_{\delta_r}}$, $C_{Y_{\delta_r}}$.

Figure 7. Continued.

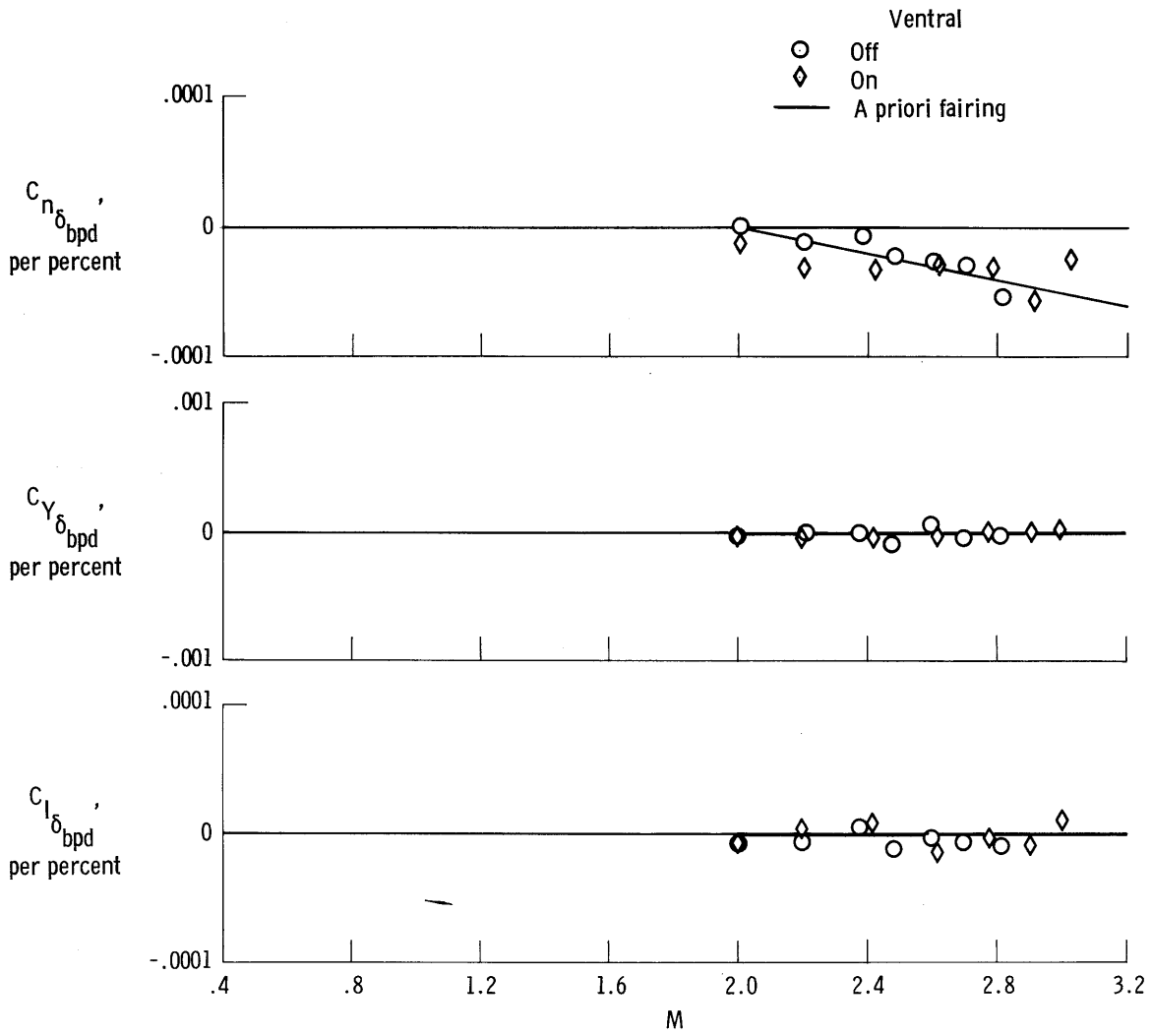

(f) $C_{n_{\delta_{bpd}}}$, $C_{Y_{\delta_{bpd}}}$, $C_{l_{\delta_{bpd}}}$.

Figure 7. Concluded.

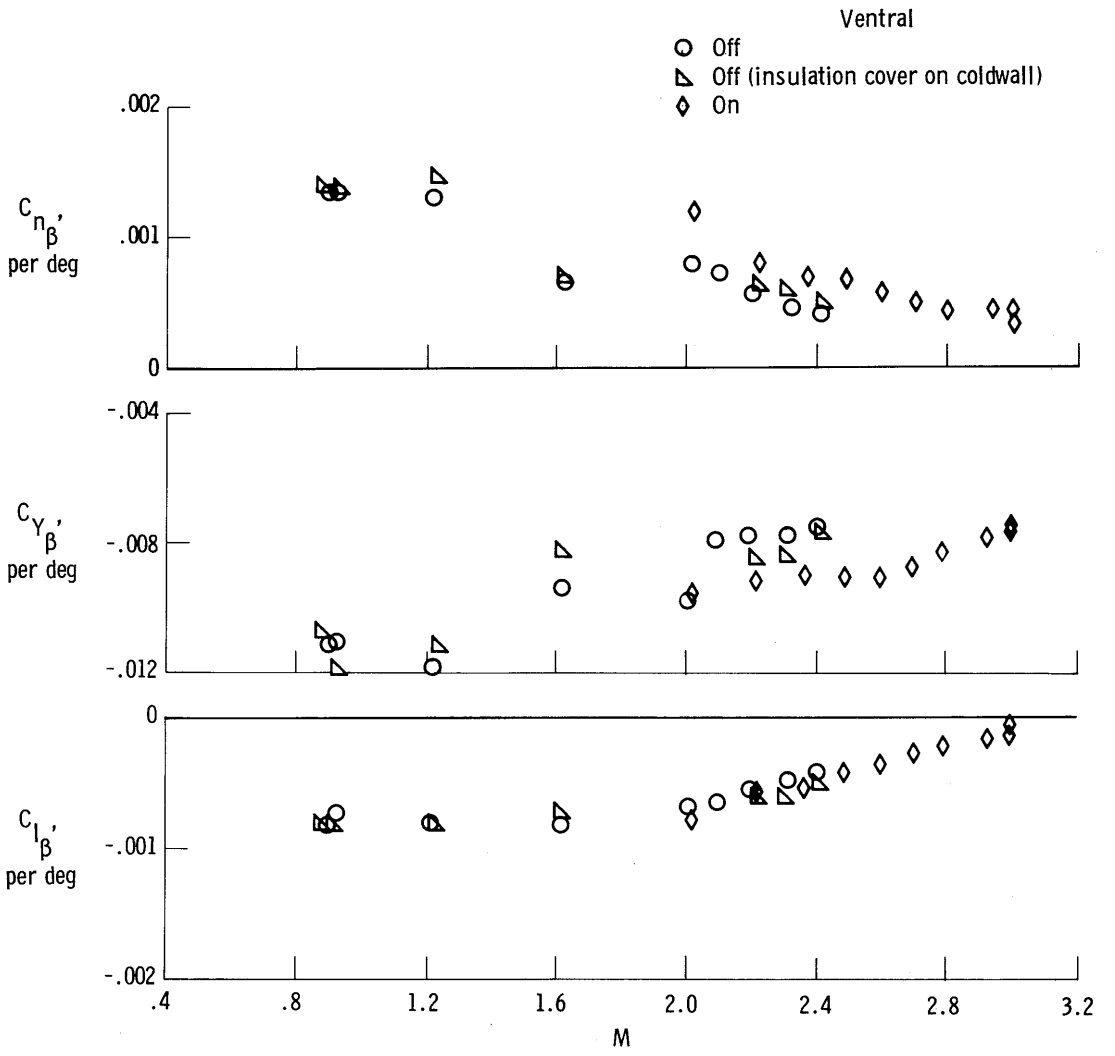

(a) C_{n_β}, C_{Y_β}, C_{l_β}.

Figure 8. Variation of coldwall-on lateral-directional derivatives with Mach number.

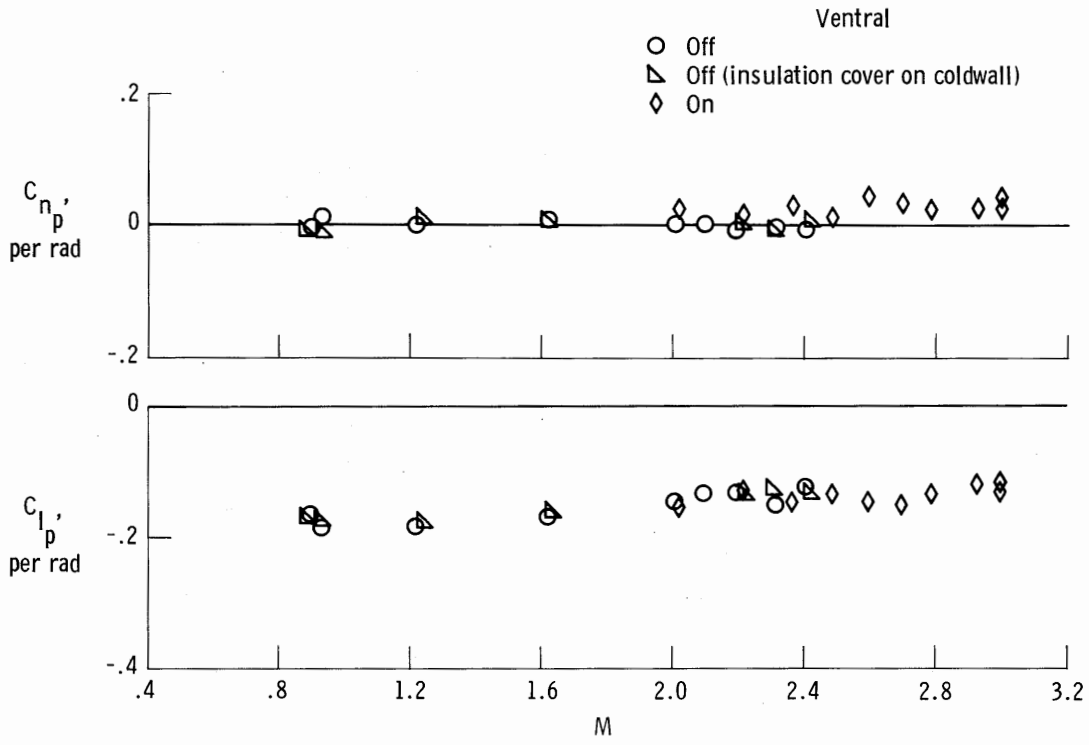

(b) C_{n_p}, C_{l_p}.

Figure 8. Continued.

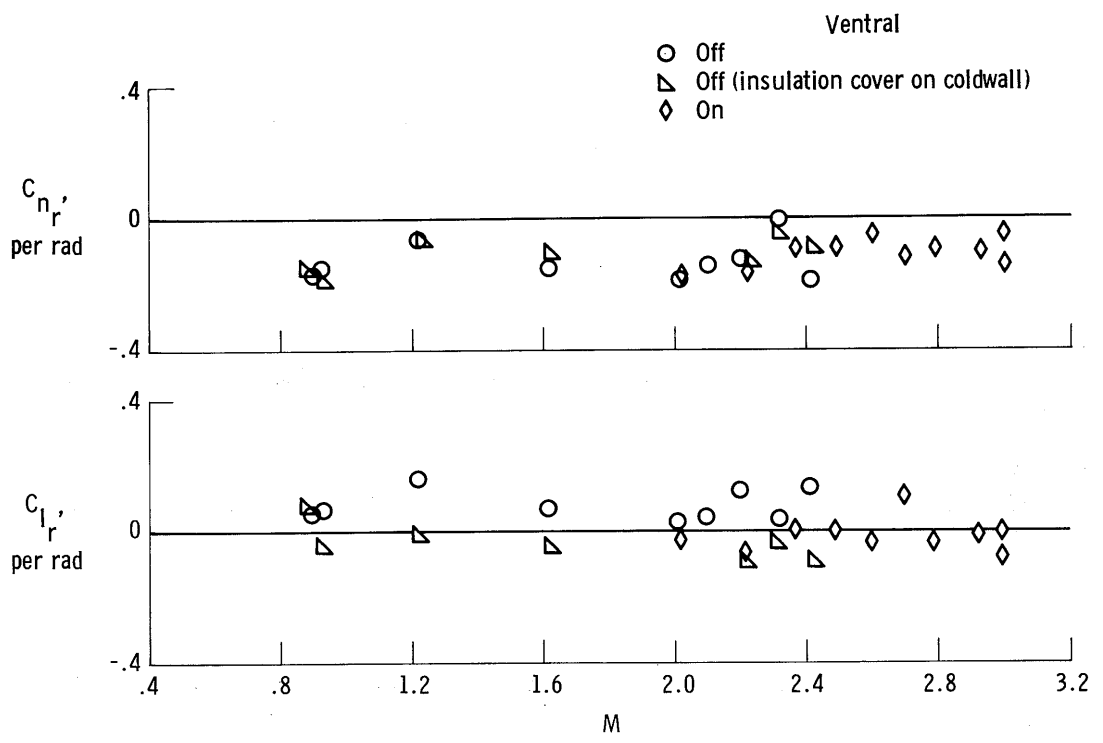

(c) C_{n_r}, C_{l_r}.

Figure 8. Continued.

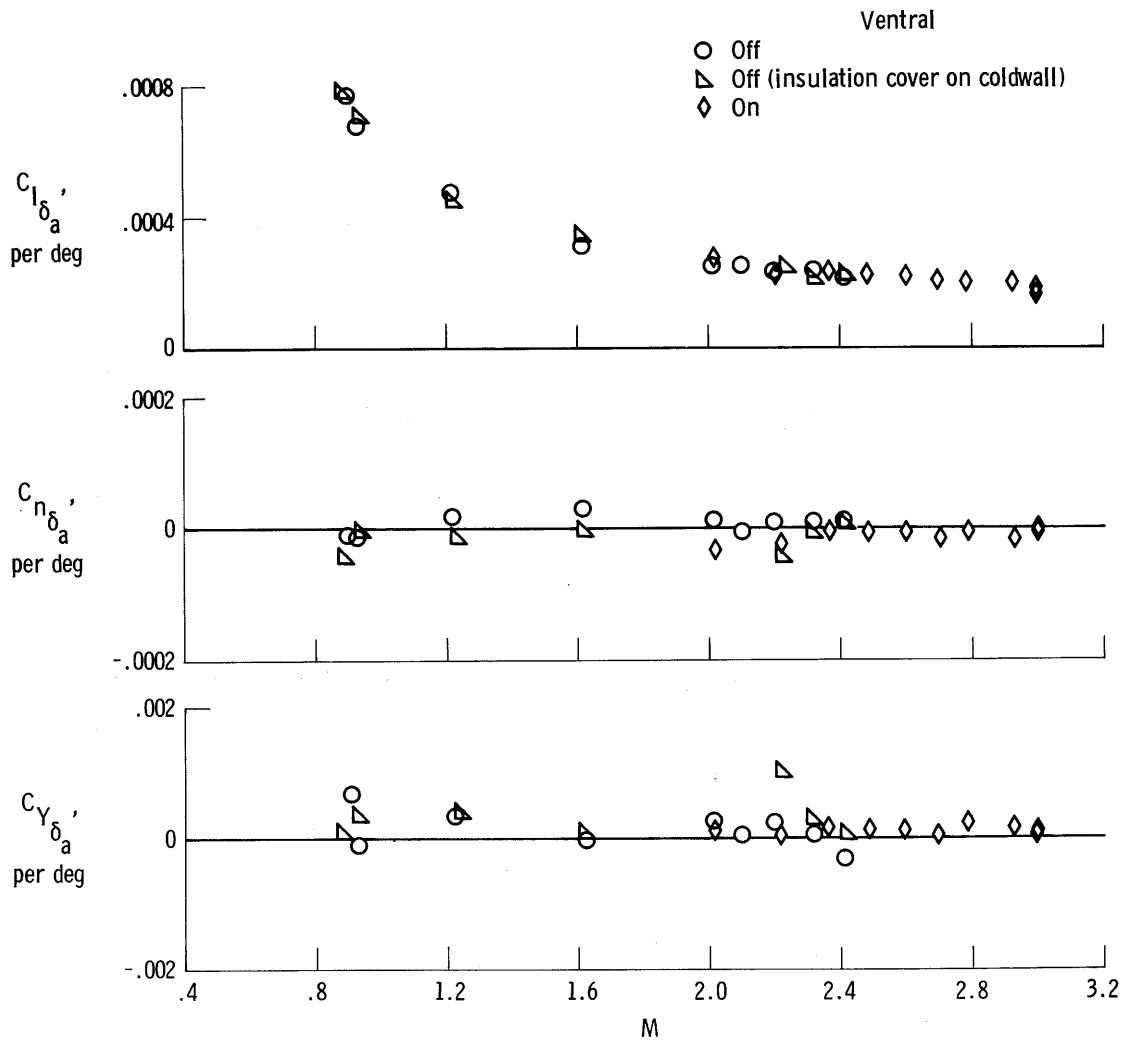

(d) $C_{l_{\delta_a}}$, $C_{n_{\delta_a}}$, $C_{Y_{\delta_a}}$.

Figure 8. Continued.

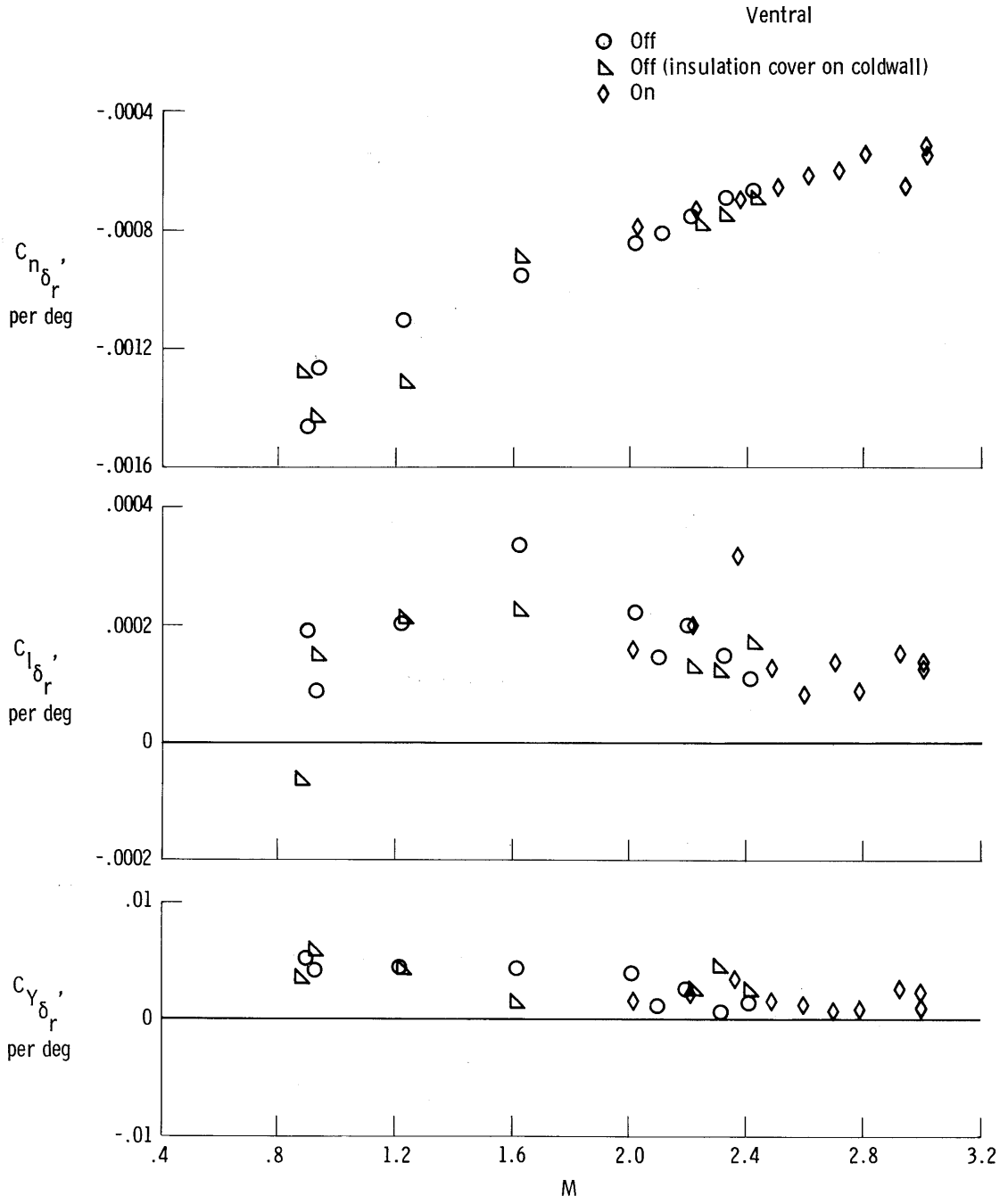

(e) $C_{n_{\delta_r}}$, $C_{l_{\delta_r}}$, $C_{Y_{\delta_r}}$.

Figure 8. Continued.

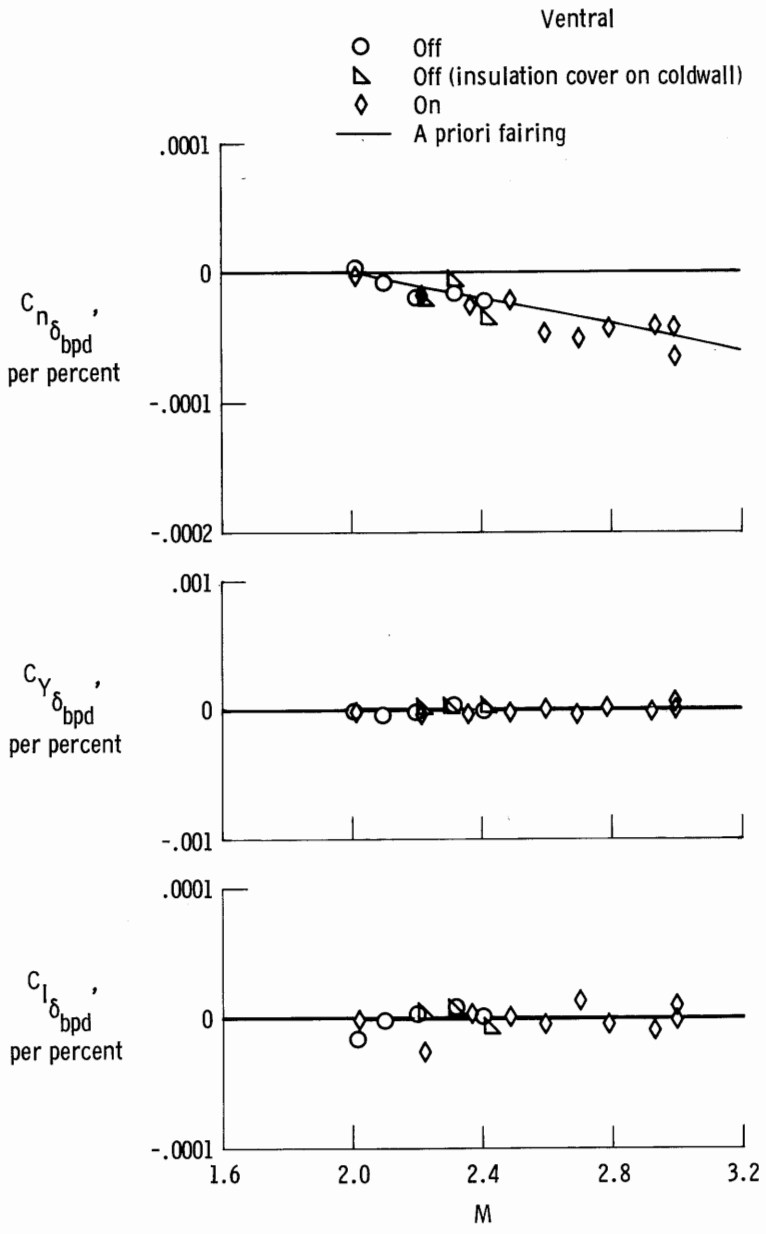

(f) $C_{n_{\delta_{bpd}}}$, $C_{Y_{\delta_{bpd}}}$, $C_{l_{\delta_{bpd}}}$.

Figure 8. Concluded.

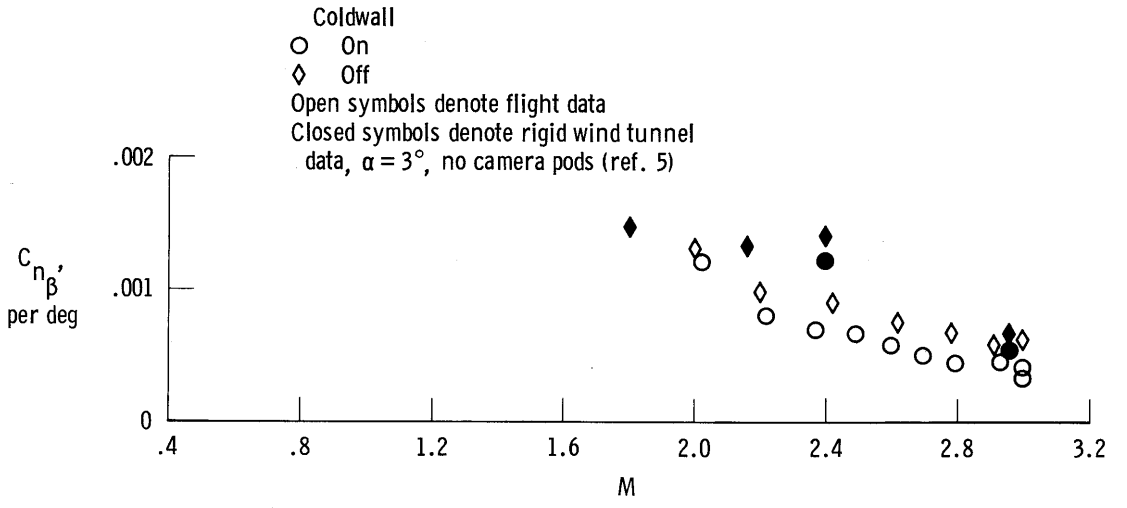

(a) Ventral on.

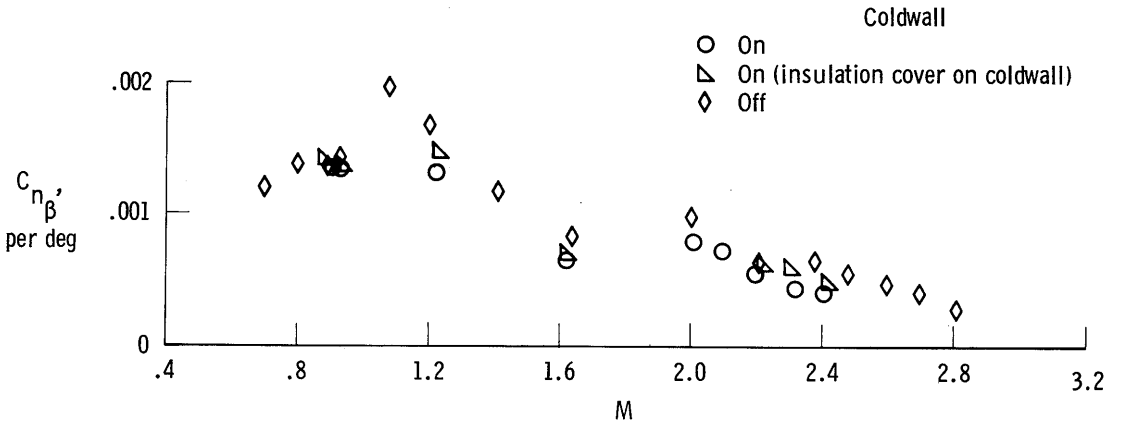

(b) Ventral off.

Figure 9. Variation of C_{n_β} with Mach number (summarized from figures 7 and 8).

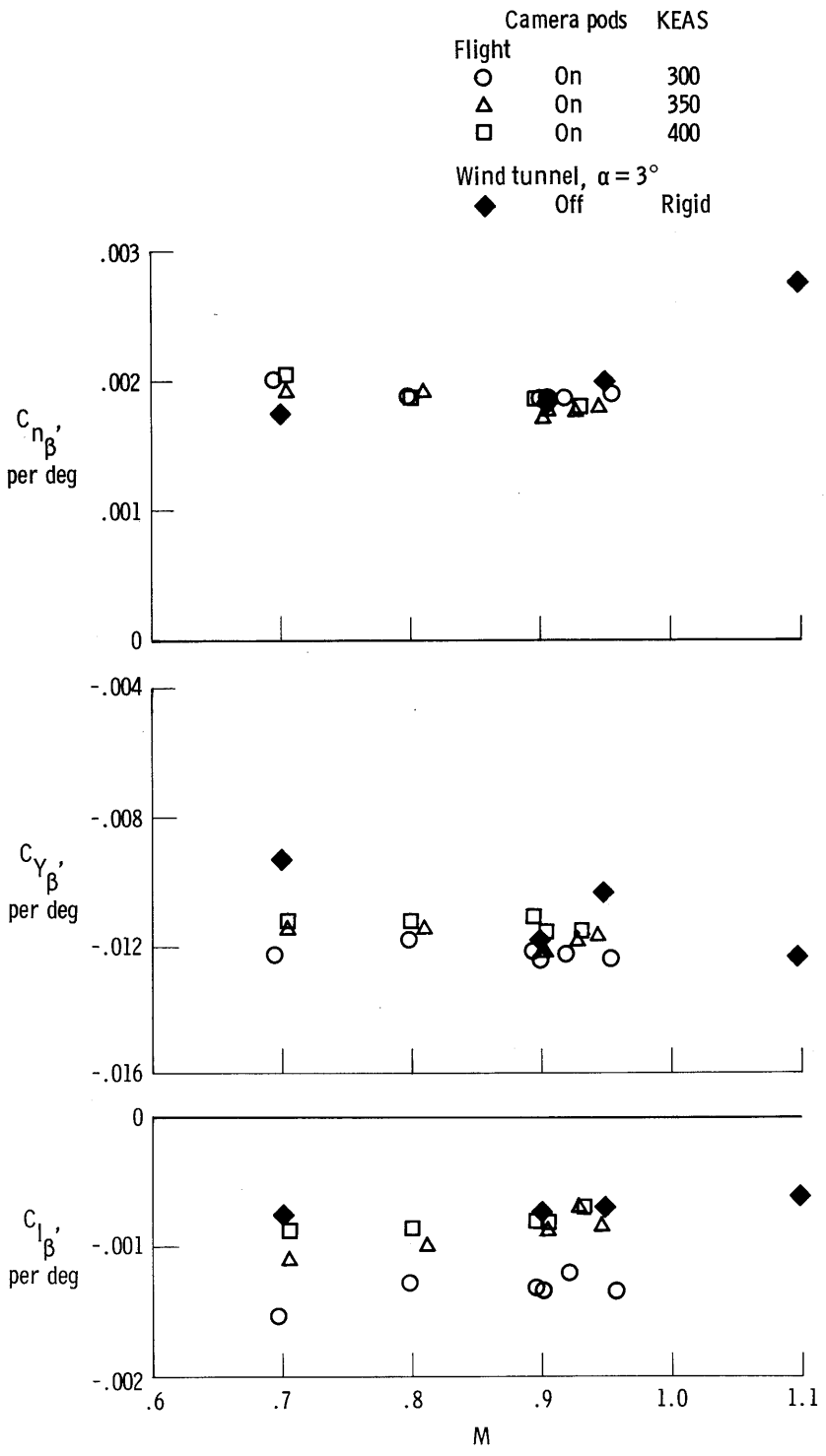

(a) C_{n_β}, C_{Y_β}, C_{l_β}.

Figure 10. Variation of subsonic lateral-directional derivatives with Mach number. Ventral on; coldwall off.

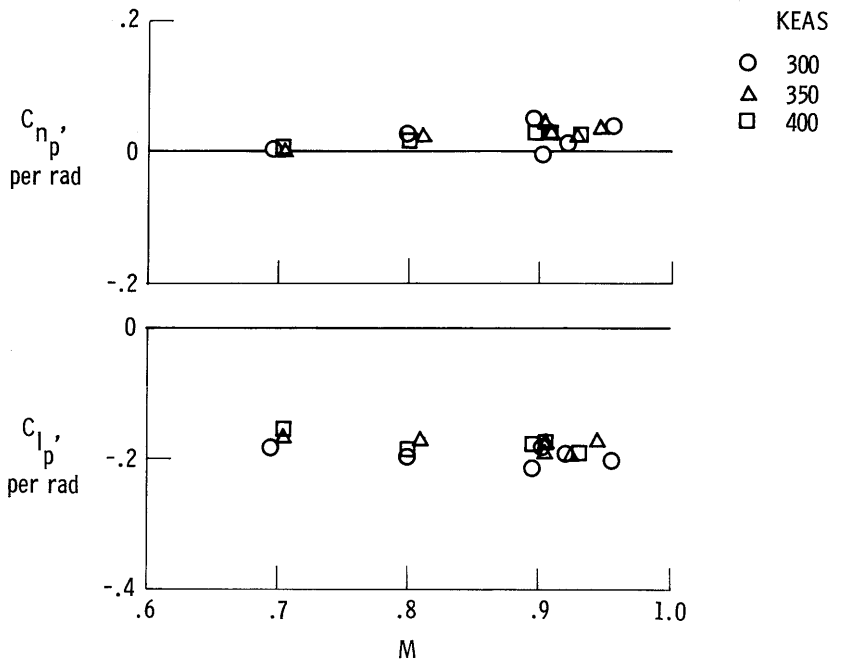

(b) C_{n_p}, C_{l_p}. *Flight data, camera pods on.*

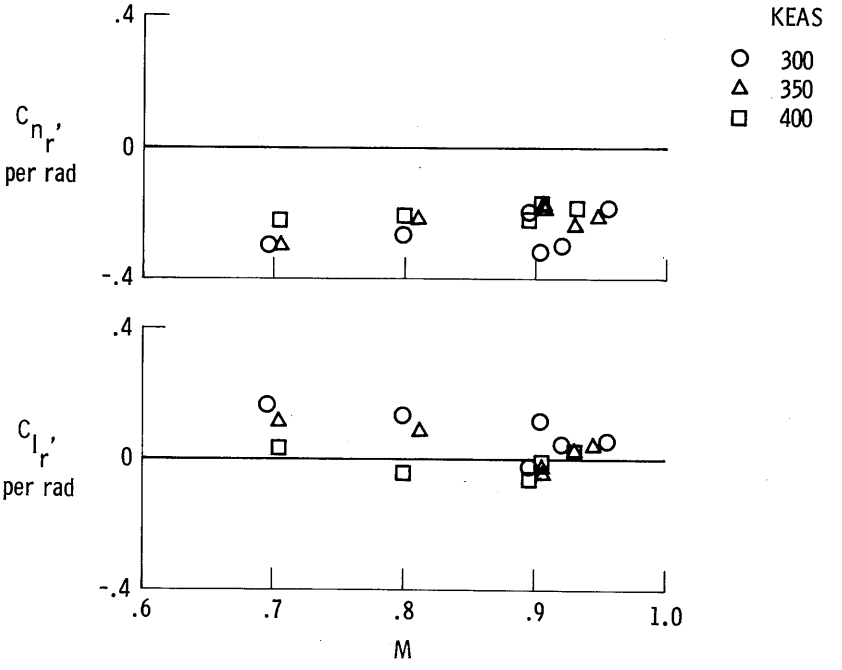

(c) C_{n_r}, C_{l_r}. *Flight data, camera pods on.*

Figure 10. Continued.

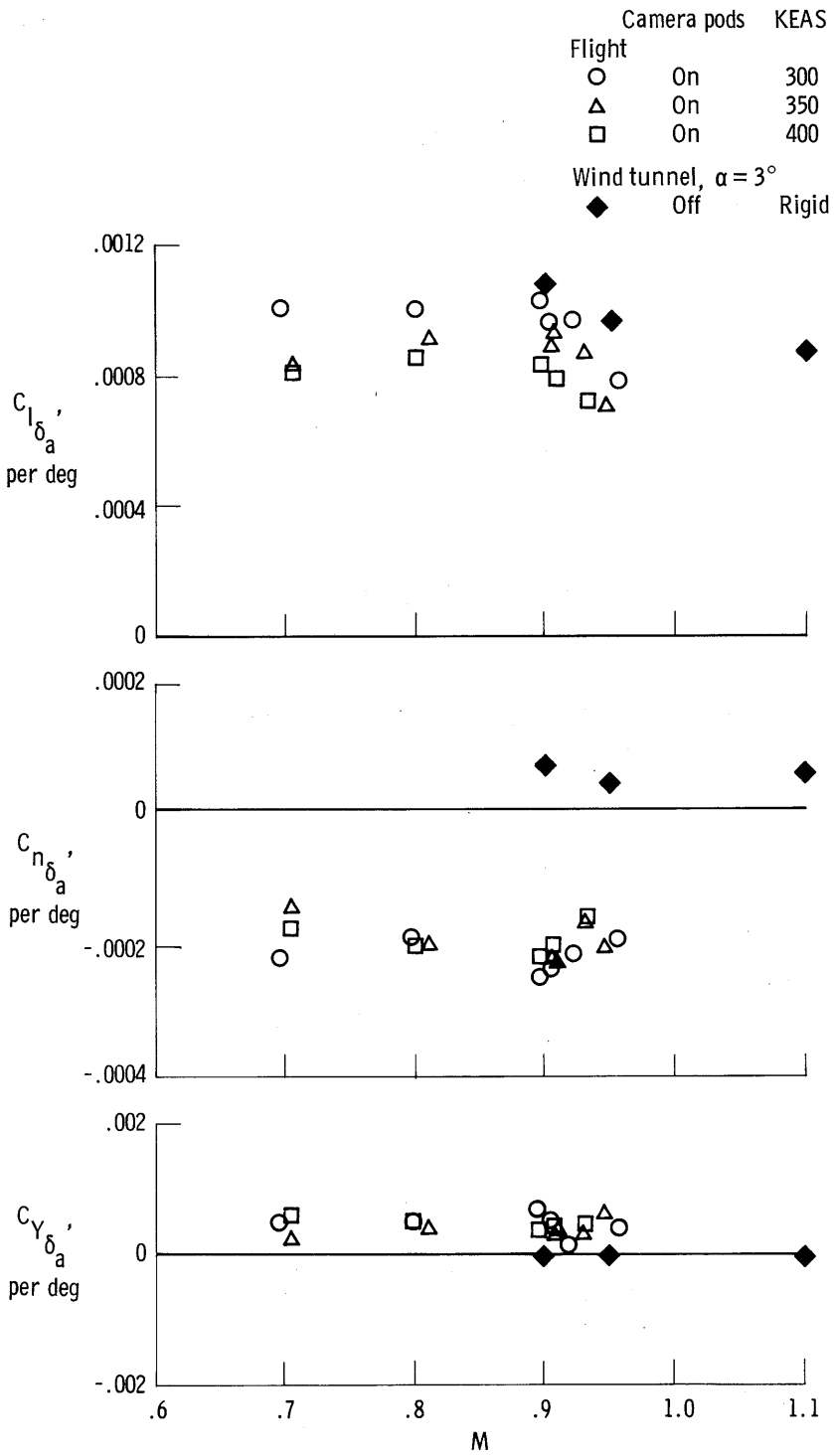

(d) $C_{l_{\delta_a}}$, $C_{n_{\delta_a}}$, $C_{Y_{\delta_a}}$.

Figure 10. Continued.

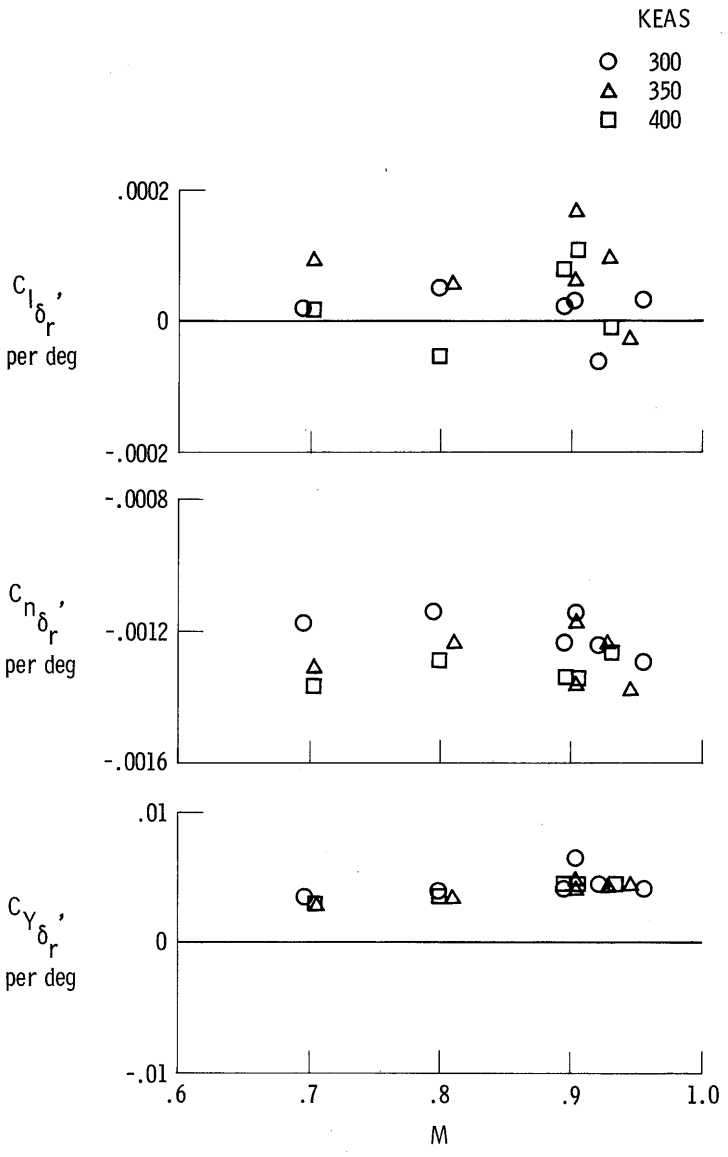

(e) $C_{l_{\delta_r}}$, $C_{n_{\delta_r}}$, $C_{Y_{\delta_r}}$. *Flight data, camera pods on.*

Figure 10. Concluded.

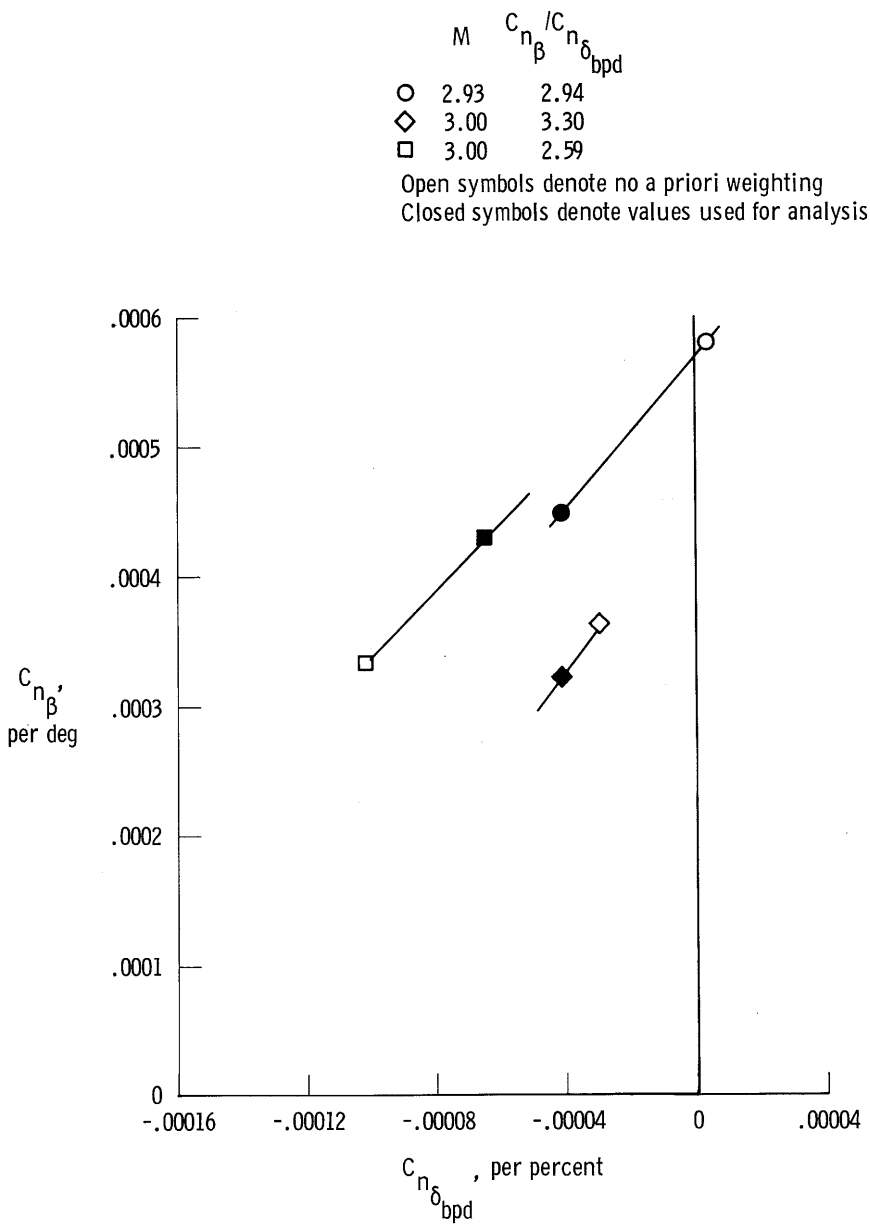

Figure 11. Variation of C_{n_β} with $C_{n_{\delta_{bpd}}}$ as a function of a priori weighting.

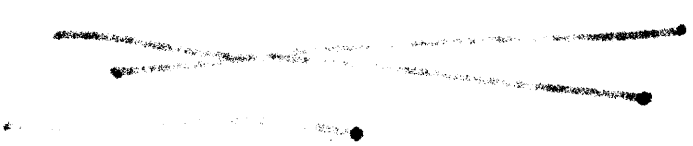

~~CONFIDENTIAL~~

1. Report No. NASA TM-72852	2. Government Accession No.	3. Recipient's Catalog No.

4. Title and Subtitle

FLIGHT-DETERMINED LONGITUDINAL AND LATERAL-DIRECTIONAL DERIVATIVES OF THE YF-12A AIRPLANE

5. Report Date: May 1978

6. Performing Organization Code

7. Author(s)

Glenn B. Gilyard (Dryden Flight Research Center) and
Donald K. Hill (Lockheed California Company)

8. Performing Organization Report No. H-988

10. Work Unit No. 516-51-04

9. Performing Organization Name and Address

NASA Dryden Flight Research Center
P.O. Box 273
Edwards, California 93523

11. Contract or Grant No.

13. Type of Report and Period Covered: Technical Memorandum

12. Sponsoring Agency Name and Address

National Aeronautics and Space Administration
Washington, D.C. 20546

14. Sponsoring Agency Code

15. Supplementary Notes

16. Abstract

Flight tests were conducted on the YF-12A airplane to document the aircraft's stability and control derivatives throughout the flight envelope. The derivatives were determined from pulse and doublet type maneuvers using a maximum likelihood estimation program.

Longitudinal derivatives are presented for Mach numbers from 0.7 to 3.0 with the ventral on and the coldwall off.

Lateral-directional data are presented for Mach numbers from 0.7 to 3.0 for all combinations of ventral and coldwall configurations. A few data are presented for a configuration with an insulation cover on the coldwall.

Propulsion system effects due to the variable inlet geometry were determined longitudinally for Mach numbers greater than 1.3 and lateral directionally for Mach numbers greater than 1.9.

17. Key Words (Suggested by Author(s))

Stability and control derivatives
Derivatives
YF-12 airplane

18. Distribution Statement

U.S. Government and Contractors Only

Category: 08

19. Security Classif. (of this report)	20. Security Classif. (of this page)	21. No. of Pages	22. Price
~~Confidential~~	Unclassified	54	

'NATIONAL SECURITY INFORMATION'
Unauthorized Disclosure Subject to Criminal Sanctions

Confidential CLASSIFIED BY Joseph E. D'Agostino EXEMPT FROM GENERAL DECLASSIFICATION SCHEDULE OF EXECUTIVE ORDER 11652 EXEMPTION CATEGORY Section 5B(2) AUTHORIZED BY DOD Directive Crown Program Classification Guide

~~CONFIDENTIAL~~

NASA-Langley, 1978

~~CONFIDENTIAL~~

~~CONFIDENTIAL~~